1993

Micro-Jansky Source Counts and Spectral Indices at 8.44 GHz

Bruce Partridge
Haverford College, bpartrid@haverford.edu

Rogier A. Windhorst

E. B. Fomalont

James D. Lowenthal

1993

Micro-Jansky Source Counts and Spectral Indices at 8.44 GHz

R. Bruce Partridge
Haverford College

Rogier A. Windhorst

Edward B. Fomalont

James D. Lowenthal

THE ASTROPHYSICAL JOURNAL, 405:498–517, 1993 March 10

MICROJANSKY SOURCE COUNTS AND SPECTRAL INDICES AT 8.44 GHz[1]

ROGIER A. WINDHORST[2]
Department of Physics and Astronomy, Arizona State University, Tempe, AZ 85287-1504
EDWARD B. FOMALONT
National Radio Astronomy Observatory,[3] Edgemont Road, Charlottesville, VA 22903-2475
R. BRUCE PARTRIDGE
Haverford College, Department of Astronomy, Haverford, PA 19041
AND
JAMES D. LOWENTHAL[4]
Steward Observatory, University of Arizona, Tucson, AZ 85721
Received 1992 June 3; accepted 1992 September 14

ABSTRACT

We used the VLA to make deep images of two $7' \times 7'$ fields at 8.44 GHz with $10''$ resolution. With an rms noise of 3.2 and 5.1 μJy, respectively, in the two fields, we compiled a catalog of 82 sources. From the complete sample of 20 sources with $S \geq 14.5$ μJy, the differential 8.44 GHz source count is $dN(S)/dS = (-4.6 \pm 0.7) \times S^{-2.3 \pm 0.2}$ Jy^{-1} sr^{-1} in the range 14.5–1000 mJy. Analysis of statistical image fluctuations from weak sources (Fomalont et al. 1993) suggests that this slope remains unchanged at $\gamma = 2.3 \pm 0.2$ down to ~ 4 μJy. The normalized differential 8.44 GHz counts are similar to those at 1.41 and 4.86 GHz. All show a similarly steep submillijansky slope, which is only somewhat flatter than that expected for a nonevolving Euclidean population ($\gamma = 2.5$).

Microjansky radio sources at 4.86 GHz have been identified with faint blue galaxies ($18 \lesssim V \lesssim 28$ mag). We argue that their expected median redshift is ~ 0.5–0.75. Hence, cosmological evolution may be needed to explain the steep slope of the microjansky counts. The 8.44 GHz counts must converge with slope $\gamma \leq 2.0$ below $S_{8.44} \simeq 300$ nanojanskys (nJy), or they would exceed the available field galaxy counts down to $V \sim 28$ mag, and they must *permanently converge* below $S_{8.44} \simeq 20$ nJy, or their integrated sky brightness would distort the observed thermal cosmic background radiation spectrum at centimeter wavelengths.

Radio spectral information is summarized for these sources between 0.33 and 8.44 GHz. The high-frequency spectral indices ($S \propto \nu^{-\alpha}$) span the range $-2 \lesssim \alpha_{8.4}^{4.9}, \alpha_{8.4}^{1.4} \lesssim +1.3$ with median $\alpha_{\rm med} \simeq 0.35 \pm 0.15$. About 40% of the sources have angular size $\Theta \geq 5''$, and the median is $\Theta_{\rm med} \simeq 2''.6 \pm 1''.4$, or $\lesssim 5$–40 kpc at the expected median redshift. The extended *steep*-spectrum sources suggest synchrotron emission in distant galactic disks, while the *extended flat-spectrum* sources may indicate thermal bremsstrahlung from large-scale star formation, both occasionally with opaque radio cores.

The estimated 31.5 GHz sky brightness from nanojansky to jansky levels is $\lesssim 36$ μK (3 σ). Even if weak radio sources cluster on scales of degrees as faint galaxies do, their *anisotropic* contribution to the *COBE* DMR experiment (with 7° FWHM beam) would not exceed ~ 1.2 μK.

Subject headings: cosmic microwave background — galaxies: evolution — galaxies: starburst — radio continuum: galaxies — surveys

1. INTRODUCTION

Deep multifrequency radio source counts down to microjansky levels are necessary to understand the cosmological evolution of radio source populations other than the classical luminous giant elliptical radio galaxies and quasars. The latter two dominate the radio source population at jansky and millijansky levels. However, below a few millijanskys, an increasing fraction of starburst, Seyfert, and normal spiral galaxies is seen (Windhorst, Dressler, & Koo 1987). Hence, systematic multifrequency surveys down to microjansky levels are needed to determine the properties and cosmological evolution of the entire radio source population, particularly for those with low radio powers. Microjansky radio surveys have been made previously at 1.4 and 5 GHz, but surveys at higher frequencies are needed to determine radio spectra and to obtain clues to the physical nature of these weak radio sources. For these reasons, this paper presents deep VLA images at 8.44 GHz of areas which have been previously surveyed at 1.41 and 4.86 GHz (and also at 0.33, 0.61, or 2.7 GHz).

Deep 1.4 GHz counts show a change in slope below a few millijanskys, equivalent to a more rapid increase in the number of faint sources (Windhorst 1984; Windhorst et al. 1985). This "upturn" was confirmed by independent surveys of the same areas (Oort & Windhorst 1985) and of different areas (Condon & Mitchell 1984; Oort 1987). Windhorst, Mathis, & Neuschaefer (1990) reviewed the 1.41 GHz counts as of 1989, which are now well constrained from over 10,000 radio sources in 24 different surveys. The upturn is visible in all survey fields that reach to well below a few millijanskys at 1.41 GHz, as well as in

[1] E-mail address for reprint requests: raw@cosmos.la.asu.edu.
[2] Alfred P. Sloan Research Fellow.
[3] The National Radio Astronomy Observatory is operated by Associated Universities, Inc., under cooperative agreement with the National Science Foundation.
[4] Currently at the Department of Physics and Astronomy, Johns Hopkins University, Baltimore, MD 21218.

recent microjansky surveys at 4.86 GHz (Fomalont et al. 1991a). This upturn cannot be easily attributed to luminous giant elliptical radio galaxies or quasars, since these objects comprise only a minority of the submillijansky sources (Windhorst et al. 1985). The steep slope of the differential submillijansky counts implies that if the majority of radio sources have $z \gtrsim 0.1$, their luminosity and/or space density likely has evolved with cosmic time. Evolving models that explain the observed submillijansky counts include normal spiral (Condon 1984, 1989) or actively star-forming galaxies (Windhorst 1984; Kron, Koo, & Windhorst 1985; Windhorst et al. 1985, 1987; Oort 1987; Franceschini et al. 1989). Models with nonevolving sources are possible if a significant fraction of the sampled population are local ($z < 0.1$) low-luminosity radio galaxies (Wall et al. 1986; Subrahmanya & Kapahi 1983).

Deep optical identification work shows that the radio source population below 1 mJy is dominated by faint blue radio galaxies (Kron et al. 1985; Windhorst et al. 1985, 1987), with median angular (radio) sizes $\Theta_{\rm med}$ of a few arcseconds (Coleman & Condon 1985; Oort et al. 1987; Oort 1988b; Windhorst et al. 1990). Their radio spectra are usually steep between 0.61 (or 1.41) and 4.86 GHz (Donnelly, Partridge, & Windhorst 1987; Oort 1988a), but often show low-frequency turnovers, mostly below 0.4 GHz (Oort 1987; Oort, Steemers, & Windhorst 1988). However, at the faintest flux-density levels ($S_{4.9} \lesssim 10$ μJy), the source properties may be somewhat different: their median angular size may become somewhat larger again, their radio spectrum flatter, and their optical counterparts optically somewhat fainter (Fomalont et al. 1991a).

The purpose of this paper is to continue the investigation of weak radio galaxy populations by extending our deep surveys to 8.44 GHz, which has become possible with the new, sensitive 3.6 cm receivers at the VLA. Our goals are (1) to measure the 8.44 GHz source counts, and compares these with the deep 1.41 and 4.86 GHz counts; (2) to study the microjansky radio source spectra by combining our 8.44 GHz survey with previous deep surveys of our fields at lower frequencies; (3) to use radio spectral and size information to constrain the nature and emission mechanism of the microjansky radio source population; and (4) to estimate the discrete radio source contribution to the *COBE*/differential Microwave Radiometer (DMR) experiment at 31.5 GHz.

In an accompanying paper (Fomalont et al. 1993; see also Fomalont 1991b), we made a statistical analysis of the 8.44 GHz image noise distribution below the current detection level, which further constrained the 8.44 GHz count down to 4 μJy. These fluctuation results are incorporated in our source counts here. Fomalont et al. (1993) also used our 8.44 GHz images to set limits to cosmic background radiation (CBR) fluctuations on 10″–80″ scales. For this, our current determination of the 8.44 GHz counts is essential to remove fluctuations caused by discrete "foreground" radio sources.

The 8.44 GHz VLA observations are described in § 2. In § 3 we describe the calibration, imaging, and subsequent processing, and in § 4 the source list, its reliability, and its completeness. In § 5 we present the millijansky 8.44 GHz source counts and discuss limits to the nanojansky counts at high frequencies. In § 6 we determine the radio spectra of weak 8.44 GHz sources, discuss the spectral index–flux density relation, discuss constraints to the nature and cosmological evolution of microjansky radio sources, and set limits to the discrete source contribution in the *COBE* DMR experiment. Our conclusions are given in § 7.

2. VLA OBSERVATIONS AT 8.44 GHz

The 8.44 GHz ($\lambda = 3.55$ cm) observations were made on eight different days from 1989 December to 1990 January with the Very Large Array in the D-configuration with 40–1000 m baselines (Thompson et al. 1980). We used the new 8.4 GHz system simultaneously at two frequencies, 8.415 and 8.465 GHz, each with two circular polarizations and 50 MHz bandwidth. The average frequency is 8.440 GHz.

We observed two fields, both studied earlier with the VLA and the Westerbork Synthesis Radio Telescope at lower frequencies (see § 6.1), which contained *no* sources brighter than 1 mJy at 6 cm (Donnelly et al. 1987) and brighter than 5 mJy at 21 cm (Windhorst et al. 1985). The "Cepheus" field is centered at R.A. $3^{\rm h}10^{\rm m}00^{\rm s}$, decl. $+80°10'00''$, and the Lynx.2 field of Windhorst, van Heerde, & Katgert (1984a)—hereafter referred to as the "Lynx field"—is at R.A. $8^{\rm h}41^{\rm m}40^{\rm s}$, decl. $+44°45'00''$ (equinox 1950.0). The field centers were selected to place known 1.4 GHz sources brighter than a few millijanskys at or near the null of the 8.44 GHz primary beam. The high declinations gave uniform and symmetric UV coverage. In total, we obtained about 63 hr of integration on the Lynx field, and about 20 hr on the Cepheus field. For each field, 25 minute integrations were alternated with 3 minute integrations on a nearby phase calibrator. The flux density calibrator 3C 286 or 3C 48 was observed at least once a day to determine the flux-density scale and polarization parameters.

In 1988 September we observed the Cepheus field for 20 hr in poor weather. Only one frequency (at 8.465 GHz) was available. After proper weighting, these earlier data were added to those obtained in 1989–1990, resulting in the equivalent of 30 hr of usable data on this field.

3. CALIBRATION AND IMAGING

3.1. *Editing and Calibration*

All data associated with shadowed antennas were removed. Individual data points in excess of 8 σ were discarded, since they are likely due to interference or hardware noise spikes. The data from correlators in excess of 10 σ—when averaged over 4 hr intervals—were removed following the procedure of Fomalont et al. (1984). In total, less than 5% of the observations were discarded. We also deleted one complete day of data in the Cepheus field—a total of 10 hr—because snow in the antennas had increased the noise level by a factor of 5.

We based the flux density calibration of the Cepheus field in 3C 48, assuming flux densities of 3.34 and 3.32 Jy at the two independent frequencies, 8.415 and 8.465 GHz, respectively. For the Lynx field, we used 3C 286 with flux densities of 5.20 and 5.18 Jy, respectively. These values are within 4% of the flux density scale of Baars et al. (1977). Since 3C 48 is a known variable on time scales of years, we used the appropriate flux density as monitored by the VLA. As phase calibrators, we observed 0212+735 and 0917+449 near the Cepheus and Lynx fields, respectively. Their assumed (equinox 1950.0) positions are R.A. $02^{\rm h}12^{\rm m}49^{\rm s}.922$, decl. $+73°35'48''.09$, and R.A. $09^{\rm h}17^{\rm m}41^{\rm s}.919$, decl. $+44°54'39''.62$, respectively, which are accurate to 0″.02.

Typical changes in antenna gain were 2% over a day, and the phase variations were less than about 10° at 1 km baselines for more than 80% of the time. There were no significant phase closure errors. These variations are sufficiently small that the sensitivity limitation of the images is receiver noise, rather than atmospheric phase variations or other instrumental changes.

At 8.44 GHz, the system sensitivity changes with weather conditions and cloud cover, and these changes were monitored from the rms noise of the data points. On several cloudy days, the rms noise was about 30% larger than on clear days. On all days the rms noise at low source elevation was larger than at transit. The UV data points were thus weighted by the inverse square of the rms noise before imaging. The effect of this is that about 25% of the data was reduced in weight to about 80% of nominal.

3.2. *Imaging and Cleaning*

Using the AIPS task MX, we combined all observations at both 8.415 and 8.465 GHz to image each field. The naturally weighted image with 10″ resolution (FWHM) had the best sensitivity. This image size was 1024 × 1024 in size with 2.″0 pixel separation. The inner quarter of the image is 17′ × 17′. This covers the entire primary-beam area at 8.44 GHz, and extends beyond the first null into the first sidelobe of the 25 m VLA antennas. Images with resolutions 18″, 30″, and 60″ were also made by weighting the visibility data more heavily at the shorter spacings. In addition to total intensity (I), images were also made in the Stokes parameters U, Q, and V to check the noise properties of the data. Images other than Stokes I are analyzed by Fomalont et al. (1993).

All images were CLEANed using the AIPS task APCLN, as described by Högbom (1974) and Clark (1980). We CLEANed down to a level of 1.5 σ with a loop gain of 0.1, which produced about 20,000 CLEAN components in the 10″ resolution image. Although negative CLEAN components were found after 1400 iterations, the additional CLEANing was necessary to remove all of the sidelobes of the real sources—and to some extent that of the noise—so that flux densities ($S_{8.44}$) and angular sizes (Θ) could be determined (for detailed test of CLEAN see Windhorst et al. 1984a; Windhorst, Mathis, & Keel 1992; Fomalont et al. 1988, 1991a).

Contour plots of the CLEANed 10″ resolution images are shown in Figures 1*a* (Lynx) and 1*b* (Cepheus). The Lynx field is the more sensitive, with an rms noise of 3.21 ± 0.05 μJy in the source-free regions. For Cepheus the rms noise is 5.08 ± 0.07 μJy. Both values are consistent with that expected from receiver noise alone. A more detailed statistical analysis of the image noise distribution is given by Fomalont et al. (1993). The absence of grating rings or other artifacts in gray-scale images (which are reproduced in Fomalont et al. 1993) of the fields shows that CLEANing has removed most of the sidelobes. The strongest sources in the images have peak flux densities above 30 σ, and their residual sidelobes are well below the noise level after CLEANing.

3.3. *Finding the Source Candidates*

More than 30 discrete sources are visible in each of the images (Figs. 1*a* and 1*b*). The brightest 8.44 GHz sources in the Cepheus and Lynx fields have flux densities of 160 and 50 μJy, respectively. Since the image noise distribution is nearly Gaussian and centered around zero, and neither image contains pixels with peak flux density $S_p \leq -4.5\ \sigma$, we expect that pixels with $S_p \geq +4.5\ \sigma$ are associated with real sources. This is therefore the completeness level for point-source detection in each field and corresponds to 14.45 and 22.85 μJy for Lynx and Cepheus, respectively.

A detailed analysis of the noise properties of all these images is presented in Fomalont et al. (1993), who reduced and analyzed the current 8.44 GHz data in two independent subsets to separate instrumentally induced noise from any real sky signal. They find that instrumental noise is spread uniformly across the images in all four Stokes parameters, and that the additional noise variance is consistent with that expected from our observed microjansky count when extrapolated below 4.5 σ with roughly the same slope (see § 5.2).

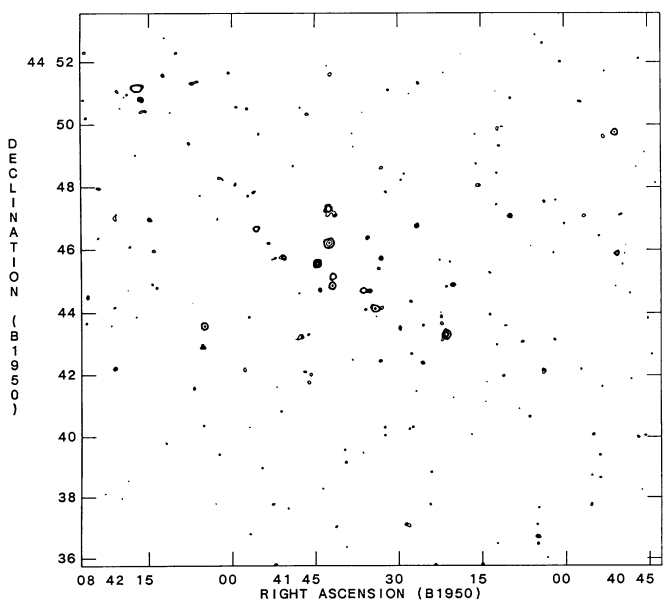

FIG. 1*a*

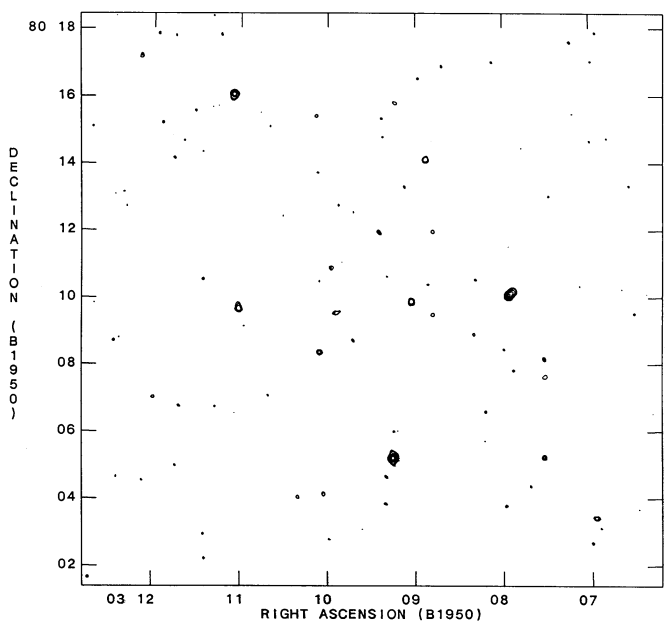

FIG. 1*b*

FIG. 1.—(*a*) Contour plot of the 8.44 GHz VLA image of the Lynx field. Contours are drawn at 3, 4, 5, 10, 15, and 20 times the rms noise level of 3.21 μJy beam^{-1}. Image FWHM = 10.″0. (*b*) Contour plot of the 8.44 GHz VLA image of the Cepheus field. Contours are drawn at 3, 4, 5, 10, 15, 20, and 25 times the rms noise level of 5.08 μJy beam^{-1}. Image FWHM = 10.″0.

TABLE 1A

CATALOG OF 8.44 GHz RADIO SOURCES IN THE LYNX.2 FIELD

Name (1)	R.A.(1950.0) (2)	Decl.(1950.0) (3)	$S_{8.44}$ (μJy) (4)	Θ (5)	χ (6)	P.A. (7)	Weight (8)	S_p (μJy) (9)	S_{int} (μJy) (10)
16V01*	$8^h40^m50^s.69$	44°45′53″.5	777	<6″.7	...	...	0.00	19.40	19.13
	0.07	0.7	218					3.30	3.30
16V02*	8 40 50.97	44 49 45.1	4516	<4.3	...	...	0.00	34.00	33.84
	0.04	0.5	1649					3.30	3.30
16V03*	8 40 53.11	44 49 36.9	1690	<10.2	...	...	0.00	13.00	12.59
	0.10	1.0	613					3.30	3.30
16V04*	8 41 3.89	44 42 7.9	1515	8.0	6″.3	117°	0.00	13.30	20.14
	0.15	1.5	591	1.5	2.1	35		3.30	5.08
16V05*	8 41 4.90	44 36 42.9	3662	6.9	3.0	61	0.00	14.00	21.96
	0.15	1.6	1667	1.5	3.0	20		3.30	5.67
16V06*	8 41 9.86	44 47 4.9	1439	<5.8	...	...	0.00	17.00	16.39
	0.08	0.8	770					3.30	3.30
16V07*	8 41 15.68	44 48 3.8	640	<12.4	...	...	0.00	13.80	13.41
	0.09	1.0	322					3.30	3.30
16V08	8 41 20.20	44 44 53.8	58.0	<9.5	...	...	1.58	16.40	16.07
	0.08	0.8	14.3					3.30	3.30
16V09	8 41 21.41	44 43 18.7	289	6.1	3.6	151	1.00	59.30	74.03
	0.04	0.4	45	0.4	0.6	10		3.30	4.13
16V10*	8 41 22.24	44 43 55.9	76.1	24.0	3.0	6	0.00	12.00	25.80
	0.28	3.0	23.1	6.0	3.0	10		3.30	8.82
16V11*	8 41 25.68	44 42 24.5	43.6	<8.4	...	...	0.00	13.00	12.59
	0.10	1.0	12.6					3.30	3.30
16V12*	8 41 26.44	44 51 21.6	744	<11.6	...	...	0.00	12.00	11.55
	0.11	1.1	284					3.30	3.30
16V13	8 41 26.66	44 46 48.3	62.1	12.6	3.0	133	2.12	14.80	23.17
	0.14	1.5	15.8	3.0	3.0	25		3.30	5.63
16V14*	8 41 28.37	44 37 6.6	818	14.0	3.0	63	0.00	13.20	23.98
	0.18	1.9	274	6.0	3.0	15		3.30	6.24
16V15*	8 41 29.67	44 43 31.0	21.4	<8.7	...	...	0.00	13.40	13.00
	0.10	1.0	5.6					3.30	3.30
16V16*	8 41 33.05	44 44 10.3	14.5	<10.0	...	...	0.00	12.60	12.17
	0.10	1.1	3.9					3.30	3.30
16V17	8 41 33.14	44 45 44.4	20.2	<6.8	...	...	5.94	16.30	15.97
	0.08	0.8	4.3					3.30	3.30
16V18*	8 41 33.15	44 48 38.0	75.3	<8.8	...	...	0.00	12.40	11.97
	0.10	1.1	23.8					3.30	3.30
16V19*	8 41 33.22	44 42 28.4	24.8	<9.7	...	...	0.00	13.00	12.59
	0.10	1.0	6.8					3.30	3.30
16V20*	8 41 33.52	44 45 25.0	14.2	<7.3	...	...	0.00	12.50	12.07
	0.10	1.1	3.8					3.30	3.30
16V21	8 41 34.19	44 44 9.1	50.4	8.5	3.0	72	2.10	35.40	44.28
	0.05	0.5	5.5	2.5	3.0	10		3.30	4.14
16V22	8 41 35.39	44 44 42.7	20.6	<9.0	...	...	5.77	19.70	19.43
	0.07	0.7	3.6					3.30	3.30
16V23*	8 41 35.61	44 46 23.1	19.2	<11.1	...	...	0.00	14.30	13.93
	0.09	1.0	4.6					3.30	3.30
16V24	8 41 36.29	44 44 43.3	32.2	<6.8	...	...	2.64	31.30	31.13
	0.05	0.5	3.7					3.30	3.30
16V25	8 41 41.84	44 45 9.4	31.5	<5.2	...	...	2.72	31.00	30.83
	0.05	0.5	3.6					3.30	3.30
16V26	8 41 41.94	44 44 52.4	35.3	<3.8	...	...	2.38	35.10	34.95
	0.04	0.5	3.6					3.30	3.30
16V27*	8 41 42.35	44 51 36.6	1153	<13.9	...	...	0.00	13.30	12.90
	0.10	1.0	478					3.30	3.30
16V28	8 41 42.51	44 46 13.5	110	10.3	6.9	140	1.53	50.20	87.64
	0.05	0.5	10	0.4	0.4	7		3.30	5.77

TABLE 1A—*Continued*

Name (1)	R.A.(1950.0) (2)	Decl.(1950.0) (3)	$S_{8.44}$ (μJy) (4)	Θ (5)	χ (6)	P.A. (7)	Weight (8)	S_p (μJy) (9)	S_{int} (μJy) (10)
16V29	$8^h41^m42^s.62$	44°47′18″.5	115	16″.8	11″.9	6°	2.10	20.40	58.51
	0.19	2.0	22	1.4	0.9	10		3.30	10.01
16V29A*	8 41 41.58	44 47 9.2	40.6	10.4	4.8	12	0.00	13.80	22.57
	0.15	1.6	10.4	1.9	2.9	22		3.30	5.45
16V30*	8 41 44.15	44 44 43.6	13.8	<5.8	...	...	0.00	13.60	13.21
	0.09	1.0	3.4					3.30	3.30
16V31	8 41 44.66	44 45 34.3	62.4	<4.1	...	...	1.53	55.50	55.40
	0.03	0.3	5.1					3.30	3.30
16V32*	8 41 46.55	44 50 19.8	851	<8.2	...	...	0.00	12.40	11.97
	0.10	1.1	471					3.30	3.30
16V33*	8 41 47.73	44 43 13.9	34.2	14.0	3.0	110	0.00	14.30	22.26
	0.14	1.5	8.4	6.0	3.0	20		3.30	5.22
16V34	8 41 50.84	44 45 45.8	31.0	<10.3	...	...	2.75	19.50	19.23
	0.07	0.7	5.9					3.30	3.30
16V35*	8 41 53.44	44 46 13.0	25.4	<8.8	...	...	0.00	12.00	11.55
	0.11	1.1	7.5					3.30	3.30
16V36	8 41 55.64	44 46 40.8	78.1	<5.1	...	...	1.37	24.60	24.38
	0.06	0.6	14.9					3.30	3.30
16V37*	8 41 57.79	44 42 12.0	79.0	<10.8	...	...	0.00	12.70	12.28
	0.10	1.1	24.6					3.30	3.30
16V38*	8 42 5.08	44 43 35.3	481	<5.2	...	...	0.00	36.10	35.95
	0.04	0.4	109					3.30	3.30
16V39*	8 42 5.36	44 42 55.5	273	<10.8	...	...	0.00	14.20	13.82
	0.09	1.0	93					3.30	3.30
16V40*	8 42 7.04	44 51 20.2	632	<16.7	...	...	0.00	14.60	19.84
	0.12	1.3	201					3.30	4.74
16V41*	8 42 12.48	44 51 35.2	576	<8.1	...	...	0.00	13.00	12.59
	0.10	1.0	195					3.30	3.30
16V42*	8 42 14.94	44 46 58.4	2314	<8.6	...	...	0.00	14.50	14.13
	0.09	0.9	1105					3.30	3.30
16V43*	8 42 16.43	44 50 49.1	958	8.1	3.1	50	0.00	17.60	22.87
	0.10	1.0	280	2.0	2.1	20		3.30	4.35
16V44*	8 42 17.18	44 51 10.3	4450	15.7	5.9	90	0.00	30.30	65.92
	0.09	1.0	1107	0.4	1.6	3		3.30	7.18
16V45*	8 42 20.76	44 51 5.5	1555	<9.9	...	...	0.00	12.60	12.17
	0.10	1.1	567					3.30	3.30
16V46*	8 42 21.17	44 42 13.6	531	<8.8	...	...	0.00	14.90	14.54
	0.09	0.9	167					3.30	3.30

An initial list of source candidates was constructed following Windhorst et al. (1984a). To find all sources brighter than the stated catalog completeness level, we used a peak-finder algorithm to search each 10″ resolution image for sources with $S_p \geq 4.0\ \sigma$ within 10′ of the field center. This area includes the first sidelobe of the 25 m VLA antennas. Components of two visibly double sources not found by this algorithm were dealt with separately, as discussed in § 4.3. Forty-six sources were found in Lynx, and 36 sources in Cepheus. All 82 sources are included in Table 1, since 8.44 GHz sources *not* in the complete sample were usually still detected in several wider area deep surveys at lower frequencies (§ 6) and are thus likely real objects. However, sources below our formal completeness level ($S_p < 4.5\ \sigma$) should not be used to derive statistical properties of the weak 8.44 GHz population.

Above the 4.5 σ level, we found 22 sources in Lynx and 11 sources in Cepheus. Of these, 14 and six, respectively, fall within the 8% attenuation contour of the VLA primary beam (see § 4.2 below). These 20 sources form our complete sample within 4′.59 radius from each 8.44 GHz field center, where the primary-beam attenuation is known to better than 14% accuracy (§ 4.2).

We also constructed images with resolutions of 18″, 30″, and 60″ (FWHM). These images have lower sensitivity for point sources but were used to search for additional low surface brightness extended sources. In particular, we looked for sources with $S_p < 4.5\ \sigma$ in the high-resolution image, but with *integrated* flux-density above the 4.5 σ catalog threshold (Windhorst et al. 1984a). No new sources were found.

4. SOURCE PARAMETERS AND THE 8.44 GHz SOURCE LIST

4.1. *Determination of Source Parameters and Their Errors*

We followed the methods of Windhorst et al. (1984a), Donnelly et al. (1987), and Fomalont et al. (1991a) to determine the

TABLE 1B

CATALOG OF 8.44 GHz RADIO SOURCES IN THE CEPHEUS FIELD

Name (1)	R.A.(1950.0) (2)	Decl.(1950.0) (3)	$S_{8.44}$ (μJy) (4)	Θ (5)	χ (6)	P.A. (7)	Weight (8)	S_p (μJy) (9)	S_{int} (μJy) (10)
17V01*	$3^h\ 6^m56^s.86$	80° 3′25″.8	2023	<11″.3	...	...	0.00	27.00	26.52
	0.31	0.8	592					5.10	5.10
17V02*	3 7 13.54	80 17 37.6	1973	<13.2	...	...	0.00	17.30	16.54
	0.47	1.2	757					5.10	5.10
17V03*	3 7 31.44	80 7 39.1	1323	<8.7	...	...	0.00	22.00	21.41
	0.37	1.0	697					5.10	5.10
17V04*	3 7 31.52	80 8 11.3	942	<6.8	...	...	0.00	21.80	21.20
	0.38	1.0	462					5.10	5.10
17V05*	3 7 31.87	80 5 15.8	1806	<9.3	...	...	0.00	24.50	23.97
	0.34	0.9	662					5.10	5.10
17V06*	3 7 52.46	80 7 50.9	261	<7.5	...	...	0.00	17.70	16.96
	0.46	1.2	94					5.10	5.10
17V07	3 7 55.09	80 10 8.2	1221	14.0	3″.0	132°	1.00	110.80	193.83
	0.19	0.5	221	2.0	3.0	10		6.50	11.37
17V08*	3 8 11.79	80 6 37.4	281	<8.0	...	...	0.00	17.30	16.54
	0.47	1.2	103					5.10	5.10
17V09*	3 8 18.58	80 10 33.8	62.4	8.7	6.1	107	0.00	16.50	23.66
	0.78	2.0	20.7	1.3	2.4	38		5.10	8.13
17V10*	3 8 20.05	80 8 56.1	49.9	<7.8	...	...	0.00	18.70	18.00
	0.44	1.1	15.0					5.10	5.10
17V11*	3 8 41.72	80 16 57.1	849	<12.8	...	...	0.00	18.00	17.27
	0.45	1.2	306					5.10	5.10
17V12*	3 8 47.95	80 9 31.9	28.0	<6.3	...	...	0.00	20.50	19.86
	0.40	1.0	7.3					5.10	5.10
17V13*	3 8 48.22	80 12 0.8	40.8	<6.6	...	...	0.00	20.30	19.65
	0.40	1.0	11.1					5.10	5.10
17V14	3 8 52.84	80 14 9.2	449	<4.5	...	...	1.00	42.00	41.69
	0.21	0.5	104					5.10	5.10
17V15*	3 8 58.26	80 16 33.8	2199	<8.8	...	...	0.00	18.50	17.79
	0.52	1.3	1109					6.00	6.00
17V16	3 9 2.57	80 9 55.2	54.0	7.5	3.4	1	3.63	36.50	47.83
	0.31	0.8	8.1	1.2	1.7	17		5.10	6.84
17V17*	3 9 14.25	80 15 50.8	1861	<13.2	...	...	0.00	20.50	19.86
	0.40	1.0	1041					5.10	5.10
17V18*	3 9 15.35	80 5 15.9	3499	7.2	3.1	168	0.00	159.00	200.44
	0.12	0.3	784	0.3	0.6	3		6.00	7.57
17V19*	3 9 19.79	80 4 41.4	758	<8.6	...	...	0.00	19.00	18.31
	0.43	1.1	376					5.10	5.10
17V20	3 9 24.89	80 11 59.3	33.6	<11.1	...	...	5.17	23.00	22.43
	0.36	0.9	7.9					5.10	5.10
17V21*	3 9 42.35	80 8 46.9	29.1	<14.1	...	...	0.00	17.50	24.68
	0.66	1.7	8.7					5.10	7.37
17V22*	3 9 54.06	80 9 35.8	43.6	17.0	3.0	101	0.00	21.60	39.17
	0.71	1.8	10.6	4.0	3.0	19		5.10	9.80
17V23*	3 9 57.63	80 10 56.4	26.2	<5.1	...	...	0.00	21.70	21.10
	0.38	1.0	6.4					5.10	5.10
17V24*	3 10 2.47	80 4 10.9	2228	<6.1	...	...	0.00	20.70	20.07
	0.40	1.0	1246					5.10	5.10
17V25	3 10 5.57	80 8 24.0	51.8	<6.0	...	...	2.57	32.00	31.59
	0.27	0.7	9.4					5.10	5.10
17V26*	3 10 8.06	80 15 28.1	1347	<6.1	...	...	0.00	19.20	18.52
	0.43	1.1	748					5.10	5.10
17V27*	3 10 20.27	80 4 5.2	3662	<7.0	...	...	0.00	19.00	18.31
	0.43	1.1	2008					5.10	5.10
17V28	3 11 1.42	80 9 43.0	293	9.5	4.4	26	1.14	37.00	54.87
	0.34	0.9	63	0.8	1.0	8		5.10	7.72

TABLE 1B—*Continued*

Name (1)	R.A.(1950.0) (2)	Decl.(1950.0) (3)	$S_{8.44}$ (μJy) (4)	Θ (5)	χ (6)	P.A. (7)	Weight (8)	S_p (μJy) (9)	S_{int} (μJy) (10)
17V29*	3^h11^m 5.02	80°16′5 ″.1	4674	<5″.3	...	...	0.00	99.50	99.37
	0.13	0.3	1072					5.10	5.10
17V30*	3 11 24.51	80 2 14.7	1126	<7.0	...	...	0.00	17.60	16.85
	0.46	1.2	412					5.10	5.10
17V31*	3 11 24.86	80 2 57.9	545	<8.4	...	...	0.00	17.60	16.85
	0.46	1.2	199					5.10	5.10
17V32*	3 11 41.64	80 6 46.7	3454	<9.2	...	...	0.00	18.00	17.27
	0.45	1.2	1813					5.10	5.10
17V33*	3 11 46.44	80 14 11.8	903	<8.4	...	...	0.00	17.80	17.06
	0.46	1.2	328					5.10	5.10
17V34*	3 11 59.71	80 7 2.0	1065	<7.9	...	...	0.00	18.50	17.79
	0.44	1.1	394					5.10	5.10
17V35*	3 12 9.12	80 17 12.6	2236	<7.8	...	...	0.00	21.00	20.38
	0.39	1.0	893					5.10	5.10
17V36*	3 12 42.72	80 1 39.9	63543	<7.9	...	...	0.00	18.70	18.00
	0.44	1.1	51205					5.10	5.10

source parameters by fitting two-dimensional elliptical Gaussians to the CLEANed images. This AIPS task IMFIT yielded the following source parameters: its (X, Y) position [converted to (R.A., decl.) following Oort & Windhorst 1985], peak and integrated image flux density (S_p and S_{int}), observed and deconvolved Gaussian major and minor axes (expressed as FWHM, the observed Gaussian major axis is referred to as a, the deconvolved Gaussian major axis as Θ), plus the sky position angle (P.A.) of Θ, as well as all their formal fitting errors. Only one out of 82 sources in Table 1 has $\Theta \gtrsim 20''$; most others have $\Theta \lesssim 10''$–$15''$ and are therefore not seen as separate double sources with our 10″ FWHM beam. They were thus fitted by *one* Gaussian component on the 10″ resolution image. Only two sources are clearly resolved into multiple components (see § 4.3), and each of their components was fitted by a single Gaussian.

The source positions in Table 1 refer to the centroid of the single Gaussian components. The quoted position error is the quadrature sum of the absolute position calibration error, and a signal-to-noise dependent error term (see Windhorst et al. 1984a). The former amounts to 0″.25 and is about the limiting positional accuracy that can be obtained at 8.44 GHz in the D-configuration. The latter is generally the dominant term (typically $\simeq 1''$).

Peak flux densities S_p were measured directly from the 10″ resolution image. The error in S_p is equal to the rms image noise. For extended sources, the integrated image flux density S_{int} has a larger error (proportional to the number of beam areas covered by the source; Windhorst et al. 1984a). The *sky* flux density of a source is equal to its integrated *image* flux density divided by the primary-beam attenuation of the individual VLA antennas at 8.44 GHz (§ 4.2). The total flux density error equals the quadrature sum of the image flux density error, the 4% calibration error in the absolute flux density scale, the uncertainty in the primary-beam attenuation, and a contribution from the nominal pointing error (see § 4.2).

Our source sizes are defined as follows. The Gaussian fitting algorithm yields the observed source major and minor axes (a and b). Compared with the true (deconvolved) FWHM source sizes, these are considerably blurred by our 10″ FWHM beam. Under the assumption that slightly resolved sources and the restoring beam are well approximated by two-dimensional elliptical Gaussians, deconvolved source sizes (major axis Θ and minor axis χ, both FWHM) and their position angle can be derived from the fitted Gaussian major and minor axes to *both* the source *and* the restoring beam, using the analytical elliptical Gaussian deconvolution method of Wild (1970). The formal fitting errors in the deconvolved source sizes are estimated by the IMFIT algorithm. These do not include systematic errors induced by the Gaussian fitting algorithm and image noise, which are discussed in § 4.3, together with upper limits to the angular sizes of unresolved sources.

4.2. *The Primary-Beam Correction*

The primary-beam sensitivity of the VLA antennas was measured by Napier & Rots (1982) at 1.462 GHz out to the 5% attenuation contour with an accuracy of 1%–2%. It was also measured by Napier (1989, 1992) at 4.885 GHz out to the first sidelobe. The VLA primary-beam attenuation could be estimated to within ~25% in the central part of the first sidelobe (Windhorst et al. 1985; Oort & Windhorst 1985). Occasionally, strong sources can be seen out to the fourth sidelobe (Fomalont et al. 1991a). Oort & Windhorst (1985) give a periodic best fit that reproduces the measurements in the main beam *and* approximates the first sidelobe (but not beyond!):

$$\mathrm{ATT}[r(\mathrm{deg}), \nu(\mathrm{GHz})] = \cos^2(109.7486 r\nu) \times \exp\left[-0.6723(r\nu)^2 - 0.8478(r\nu)^4\right], \quad (1)$$

where ATT ≤ 1. This fit also reproduces the recent Napier (1992) 4.885 GHz measurement within 3%–5% out to 10 dB. Hence, for our purposes, the VLA primary-beam shape scales well enough with wavelength that we may extrapolate equation (1) to 8.44 GHz. At 8.44 GHz the first null occurs at 5′.92. The peak of the first sidelobe occurs at 8′ from the field center and has ATT $= 0.027 \pm 0.006$.

For sources in the complete sample (within the 8% attenuation level at 4′.59 radius), the accuracy of the 8.44 GHz

primary-beam correction increases monotonically from ~3% within 3′ from the field center to 14% at 4.′59 radius, beyond which the primary-beam uncertainty increases steadily out to the first null. Following Windhorst et al. (1984a), the derivative of equation (1) multiplied by the rms pointing error of the VLA antennas ($\lesssim 10''$ during our night-time observations) yields the flux density error induced by the rms pointing error.

4.3. *Correction for Biases in the Source Parameters*

In addition to the primary-beam correction, the determination of true sky flux densities ($S_{8.44}$) from image peak flux densities (S_p) requires several other corrections for systematic effects (see Windhorst et al. 1984a; Fomalont et al. 1991a). These are described below.

4.3.1. *Delay Smearing by the* 50 MHz *Bandwidth*

At 8.44 GHz, the 50 MHz bandwidth broadens a source in the radial direction by about 0.006 of its distance from the field center. At 4.′59 from the field center, the FWHM broadening is about 1.″6 and decreases the peak flux density S_p of a point source by $\lesssim 16\%$. However, since the total image flux density $S_{\rm int}$ is preserved to first and second order by the elliptical Gaussian fitting routine (Windhorst et al. 1984a), no corrections for bandwidth smearing were applied to the integrated source flux density. Neither did we correct the measured source angular size for delay broadening, since this effect is always less than the smallest detectable angular size (which is about 3″; § 5.1).

4.3.2. *Deconvolved Source Sizes and Resolution Bias*

Even in the absence of noise, an elliptical Gaussian fitting routine will systematically overestimate the true (deconvolved) angular size of weak sources (by up to a factor of 2 for 5 σ sources; Windhorst et al. 1984a). Because the shape of the natural weighted VLA beam makes this correction rather uncertain, we have not applied any statistical corrections to the deconvolved source sizes in Table 1. This must be kept in mind when considering the angular size distribution of § 5.1. We believe that all sources with a quoted angular size in Table 1 are indeed extended, as can be seen in Figure 1. For sources with a signal-to-noise ratio (=ratio of peak flux density S_p to rms image noise σ) of 5, the minimum resolvable source size is about 10″. For sources with $S_p/N = 25$ the resolvable size limit is about 3″. For unresolved sources, we provided 1.5 σ upper limits to Θ using the appropriately scaled expressions of Windhorst et al. (1984a).

The source counts still need to be corrected for missing faint low surface brightness sources that have peak flux densities S_p below the catalog threshold but integrated image flux densities $S_{\rm int} \geq 4.5\,\sigma$. This is described in § 5.1.

4.3.3. *Noise Bias in the Flux Density Estimates*

In the presence of noise, elliptical Gaussian source-fitting routines tend to overestimate the observed parameters of faint sources, such as peak and integrated flux density, and deconvolved source size (overestimation of the latter occurs *in addition* to that induced by the algorithm itself, as described in § 4.3.2). For a 5 σ source, this "noise bias" can produce flux density errors as large as 10%–20% in the fitted source peak flux density S_p (Windhorst et al. 1984a). The original noise-bias corrections for a Westerbork-like restoring beam (a Bessel function) were somewhat overestimated (Oort 1987; Windhorst et al. 1990) and are also not applicable to the more complicated shape of the natural-weighted VLA beam (Windhorst et al. 1985). We therefore applied a 3 times smaller correction for noise bias than that of Windhorst et al. (1984a). Our number of sources is sufficiently small that corrections for both resolution and noise bias are smaller than the statistical errors in the source counts (§ 5.2).

Out to the 8% attenuation contour, the VLA primary beam contains ~3000 independent beam areas. Hence, the 4.5 σ cutoff in S_p will introduce much less than one spurious source in the catalog. In the presence of noise bias, some sources with $S_p = 4.0\,\sigma$ intrinsically may show up with $S_p \geq 4.5\,\sigma$ in the image, but even at the 4.0 σ level less than one spurious source is expected.

4.3.4. *Confusion by Weaker Nearby Sources (Population Bias)*

Blending of sources is a more difficult problem at microjansky levels. This was addressed by Fomalont et al. (1991a), who use higher resolution 4.86 GHz VLA data and ultradeep CCD images to disentangle the sources in their nearly confusion-limited 4.86 GHz images. Since our 8.44 GHz source density is about half their 4.86 GHz source density at a given flux density S_ν (§ 5.2), blending is less important in our survey, which is limited by instrumental resolution, and not yet by confusion. We compared the surface brightness distribution in high- and low-resolution images for two possibly confused source pairs in the center of the Lynx field (16V16+16V21; 16V29+16V29A). Our best guess is that 16V16 and 16V21 are probably two unrelated sources (no low surface brightness emission seen in between the sources, and no optical identification on the Mayall 4 m plates of Windhorst, Kron, & Koo 1984b), while 16V29 and 16V29A belong to *one* physical source identified with a bright disk galaxy on those 4 m plates. Higher resolution radio images and deeper optical identifications than in Windhorst et al. (1984b) are needed to address these two cases in detail.

4.4. *The* 8.44 GHz *Catalog*

Table 1A gives the 8.44 GHz catalog for the Lynx field, and Table 1B that for the Cepheus field. The catalog contains 82 sources with $S_p > 4.0\,\sigma$ within 10′ radius from the field center. This limit corresponds to 12.8 and 20.3 μJy in the Lynx and Cepheus fields, respectively. Cataloging sources at this depth ensures that all real sources with $S_p > 4.5\,\sigma$ are found. The complete sample includes only about one-quarter of these 82 sources: within the 8% primary-beam contour (4.′59 radius), the Lynx field contains 14 sources with $S_p > 14.45$ μJy (4.5 σ), and the Cepheus field contains six sources above 22.9 μJy. The sources are numbered in order of right ascension with prefix 16V or 17V, indicating the VLA survey number. Table 1 is organized as follows:

Column (1).—The source name. Sources with an asterisk are *not* in the complete sample.

Columns (2) and (3).—The right ascension and declination (equinox 1950.0) with their 1 σ errors.

Column (4).—The integrated sky flux density ($S_{8.44}$), corrected for primary-beam attenuation and noise bias with its 1 σ error.

Columns (5)–(7).—The *deconvolved* Gaussian source size (FWHM) in arcseconds. For resolved sources, we give both the deconvolved Gaussian major and minor axes (Θ and χ, respectively), and the position angle (P.A.) of Θ (in degrees, north through east). For unresolved sources, we give 1.5 σ upper limits to Θ only.

Column (*8*).—The weight of the source in the 8.44 GHz counts (see § 5).

Column (*9*).—The measured peak flux density (S_p) on the 10″ resolution image, and its 1 σ error ($\sigma \simeq$ rms image noise), both without any corrections.

Column (*10*).—The resulting integrated flux density (S_{int}) on the 10″ resolution image, and its 1 σ error.

5. SOURCE COUNTS

From the complete sample in Table 1, we can determine the source counts in the range 14.5–1000 μJy. Since the source sample is defined in terms of peak flux density (S_p) in the 10″ resolution image, several corrections are required to transfer the *observed* surface density in the image to a *true* surface density on the sky. Some corrections are well determined (VLA primary-beam sensitivity; see § 4.2), but others are more uncertain (e.g., blending of discrete sources and instrumental broadening; see § 4.3). From the *observed* angular size distribution of weak sources, we can estimate their true angular size distribution, and then determine a source count corrected for missing low surface brightness sources.

5.1. *Angular Size Distribution and Resolution Correction*

Weak extended sources may have a *peak* flux density S_p below the 4.5 σ catalog threshold, yet still have *integrated* flux densities S_{int} above the completeness limits of our catalog. The number of "missing" sources can be estimated if both the surface density and the angular size distribution of weak radio sources (with $S_{8.44} = 5$–20 μJy) are known, following the procedure of Windhorst et al. (1984a, 1990).

The angular size distribution of sources in the deep 8.44 GHz catalog is given in Table 2. Nearly half of the sample, eight of the 20 sources, are resolved by the 10″ FWHM beam and have angular sizes $\geq 5''$. The accuracy with which a source's angular size can be determined depends on its peak signal-to-noise ratio S_p/N, and will be affected by image noise (§ 4.3.3; Windhorst et al. 1984a) and/or blending with nearby weaker sources (§ 4.3.4; Fomalont et al. 1991a). It is therefore difficult to interpret our angular size distribution unambiguously, also because the statistics are small and the beam size is 10″ FWHM. If we conservatively take 10″ as the minimum angular size which could be determined for *all* sources in the complete catalog, we find four out of 20 sources (or 20%) greater than this limit. Within the statistical errors, this fraction could be in the range 10%–30%. Equation (2) of Windhorst et al. (1990) gives an analytical expression for the flux density–dependent *integral* angular size distribution of radio sources down to $S_{1.4} \sim 0.4$ mJy. If the shape of their angular size distribution holds down to our 8.44 GHz flux density limit (equivalent to $S_{1.4} \gtrsim 0.05$ mJy), this 10%–30% fraction implies that the median angular size would be in the range $\Theta_{med} = 1''.4$–$4''.1$. The actual observed 20% fraction implies a formal value of $\Theta_{med} = 2''.6 \pm 1''.4$. Since the Gaussian fitting algorithm—even in the absence of noise—overestimates FWHM source sizes (see § 4.3) by as much as a factor of 2, the actual value of Θ_{med} of microjansky sources is expected to be $\lesssim 2''$, consistent with the $\Theta_{med} \simeq 1''.3$ value found by Fomalont et al. (1991a) for 4.86 GHz sources of similar flux densities.

TABLE 2

ANGULAR SIZE DISTRIBUTION OF MICROJANSKY SOURCES AT 8.44 GHz

NUMBER OF SOURCES	RANGE OF Θ			
	$<5''$	$5''$–$10''$	$10''$–$15''$	$>15''$
Observed	12	4	3	1
Predicted (if median = 2″.6)	12.9	3.0	1.5	2.6

NOTES.—About 40% of sources have $\Theta > 5''$, and 20% have $\Theta > 10''$, consistent with a Θ_{med} range of $1''.4$–$4''.1$ with a likely value of $2''.6 \pm 1''.4$. The bottom line shows the predicted distribution (from eq. [2] of Windhorst et al. 1990 with $\Theta_{med} = 2''.6$).

Here we address what fraction of sources has been missed by the 10″ FWHM beam, given the flux density–dependent angular size distribution, and how this affects the resolution correction to the microjansky source counts. To illustrate the problem, Figure 2 shows the median angular size Θ_{med} versus 1.41 GHz flux density for a wide range of low-frequency surveys with sufficiently high resolution that Θ_{med} could be determined. All data points with $S_{1.4} \gtrsim 0.4$ mJy come from published low-frequency surveys (primarily at 408 MHz or 1.4 GHz) from the literature compilation of Windhorst et al. (1990). Values for Θ_{med} are also plotted for the deepest two high-frequency surveys VLA available: the 4.86 GHz survey of Fomalont et al. (1991a) and the current 8.44 GHz survey. The flux density scales of surveys below 1.41 GHz were transformed to 1.41 GHz with the *low*-frequency median spectral index (α_{med}) versus flux density relation of Windhorst et al. (1990); those of the two high-frequency surveys were transformed to 1.41 GHz with the *high*-frequency α_{med} versus flux density relation of § 6.3. The dotted line for $S_{1.4} \gtrsim 1$ mJy indicates the steady decline of Θ_{med} with decreasing 1.4 GHz flux density as discussed by Oort (1987) and Windhorst et al. (1990). Our 8.44 GHz survey and the Fomalont et al. (1991a) 4.86 GHz survey suggest that below $S_{1.4} \lesssim 0.3$ mJy the value of Θ_{med} may level off to $1''.5$–$2''$. The two high-frequency surveys have at least 10–100 times better surface brightness sensitivity than the low-frequency surveys, so that the selection of flat spectrum compact radio cores at higher frequencies should not significantly affect the value of Θ_{med} (extended emission was often seen in these high-frequency surveys, and their angular size definition was the same as for the low-frequency surveys). The angular size distribution of Table 2 is consistent with $\Theta_{med} \simeq 2''.6 \pm 1''.4$, thus extending the flux density–dependent angular size distribution of Windhorst et al. (1990; their eqs. [1] and [2]) to lower flux densities. Given that our Θ_{med} value may be overestimated by the algorithm and noise (see above), Figure 2 suggests that the true median angular size of microjansky sources is not likely to exceed $\sim 2''$. The shape of the angular size distribution in Table 2 is similar to that predicted by equation (2) of Windhorst et al. (1990), which only has a 20% tail for $\Theta > 10''$. Combination of Figure 2 and Table 2 thus suggests that the number of sources missed by our 10″ FWHM beam must be small ($\lesssim$20%, or less than four out of 20 sources in the complete sample). This is confirmed by the fact that our low-resolution images (with 18″, 30″, and 60″ FWHM) did not show any new sources (§ 3.3).

To estimate the resolution correction for "missing" extended sources quantitatively, we did Monte Carlo simulations that randomly populated the primary beam with sources using the angular size distribution of Windhorst et al. (1990) and the Θ_{med} versus flux density relation of Figure 2. We explored the range of $\Theta_{med} = 1''.4$–$4''.1$. Details of the procedure are given in Fomalont et al. (1991a for 4.86 GHz; 1993 for 8.44 GHz). When $\Theta_{med} = 3''.5$ is used, these simulations show that there is a 40% chance of missing a source with integrated flux density of 18 μJy, decreasing to 12% for a source with $S_{int} = 35$

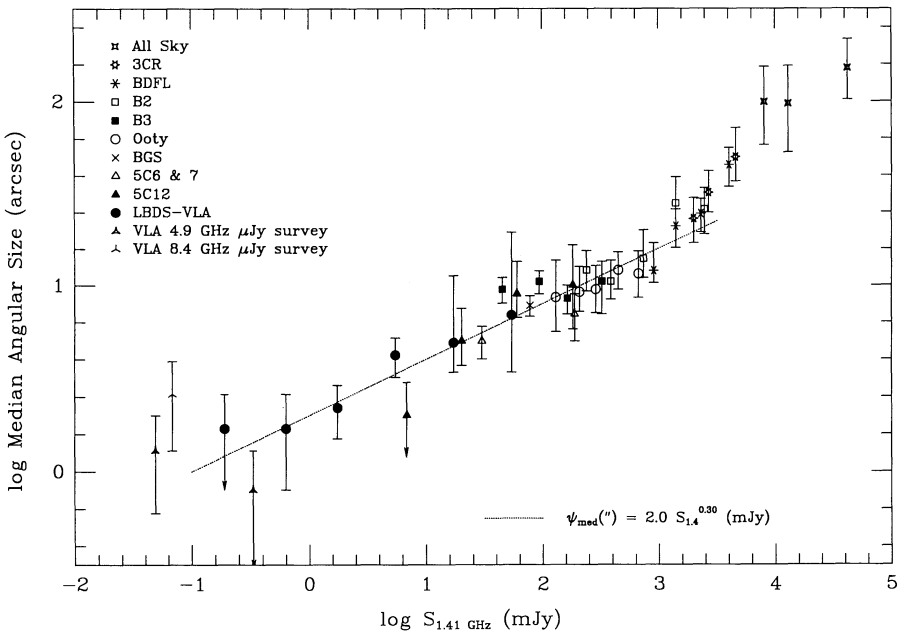

FIG. 2.—Median angular size, Θ_{med}, vs. 1.41 GHz flux density relation for previous low-frequency surveys (points with $S_{1.4} \gtrsim 0.4$ mJy), and for the current ultradeep VLA survey at 8.44 GHz, as well as for that of Fomalont et al. (1991a) at 4.86 GHz. Flux densities of all surveys were transformed to 1.41 GHz using the relations of Figs. 5*a* and 5*b*, as explained in § 6.3. The dotted line is eq. (1) of Windhorst et al. (1990). For further details see § 5.1.

μJy. Because our 10″ FWHM beam is much larger than the likely value of Θ_{med}, these fractions only drop slightly for $\Theta_{med} = 2\farcs0$, to 25% and 8%, respectively. Hence, although the value of Θ_{med} itself is uncertain by a factor of 2, the resulting relative error in (1 + the resolution correction) applied to the source counts is only ~10%, much less than the statistical error in the source counts (§ 5.2)! The adopted value of Θ_{med} ($\simeq 2\farcs6 \pm 1\farcs4$) is thus not critical to the current 8.44 GHz resolution correction. Note, however, that this is not true for the brighter surveys, which generally have $\Theta_{med} \simeq$ $FWHM_{beam}$, nor will it be true in future for microjansky surveys with much higher resolution than ours.

5.2. *The Resulting* 8.44 GHz *Counts*

Table 3 gives the resulting 8.44 GHz source counts. Column (1) gives the adopted flux density intervals such that each bin has about an equal number of sources—except for the brightest one. The latter may be incomplete because the fields were selected to have no sources stronger than a few millijanskys at 1.41 and 4.86 GHz. The lowest flux density interval was chosen between 14.5 and 22.9 μJy. This bin is populated only by the Lynx field, since the completeness limit of the Cepheus field is 22.9 μJy. Column (2) gives the average flux density (weighted with the count slope $\gamma = 2.3$) in each interval. Column (3) gives the observed distribution of peak flux densities, n_P, for the 20 sources in the complete sample. Column (4) gives the distribution of the integrated image flux density, n_I. Column (5) gives the source count based on integrated image flux densities (S_{int}), corrected for resolution bias (see § 5.1). Column (6) gives the average weight of sources that corrects for the limited visibility in peak flux density within the VLA primary beam. Column (7) gives the number of observed sources with integrated sky flux densities. Column (8) gives the corresponding source count based on integrated sky flux densities ($S_{8.44}$), corrected for

TABLE 3

THE 8.44 GHz RADIO SOURCE COUNT AT MICROJANSKY LEVELS

8.4 GHz Flux Range (μJy) (1)	$\langle S_{8.4} \rangle$ (μJy) (2)	n_P (3)	n_I (4)	n_{Ir} (5)	⟨WT⟩ (6)	n_S (7)	n_{Sr} (8)	n_{Eucl} (9)	n_{Sr}/n_{Eucl} (10)
100.0–2000.0	330.0	1	1	1.0	1.30	6	6.6	(3.6/1.30) × 2 = 5.54	1.19 (0.49)
50.0–99.9	64.3	3	5	5.0	2.13	7	8.1	(6.5/2.13) × 2 = 6.11	1.32 (0.51)
22.9–49.9	33.1	10	10	12.2	3.13	5	7.6	(22.6/3.13) × 2 = 14.44	0.53 (0.24)
14.5–22.8	19.2	6	4	7.0	5.85	2	2.9	(32.4/5.85) × 1 = 5.53	0.52 (0.37)

NOTE.—$\langle S_{8.4} \rangle$: average 8.44 GHz flux density of bin (μJy), using differential count slope $\gamma = +2.3$; n_P: number distribution of peak map flux density at 10″ resolution; n_I: number distribution of integrated map flux density; n_{Ir}: number distribution of integrated map flux density, corrected for resolution; ⟨WT⟩: average weight of sources in flux density bin (= reciprocal of detectable area); n_S: differential number distribution of integrated sky flux density; n_{Sr}: differential number distribution of integrated sky flux density, corrected for resolution; n_{Eucl}: expected differential Euclidean number distribution of integrated sky flux density [derived from the integral $N(>S) = S^{-1.5}/1.5$, as in Aizu et al. 1987] per steradian per flux unit corrected for ⟨WT⟩ (col. [6]) and for the number of contributing fields; n_{Sr}/n_{Eucl}: resulting normalized differential source count (with estimated rms error).

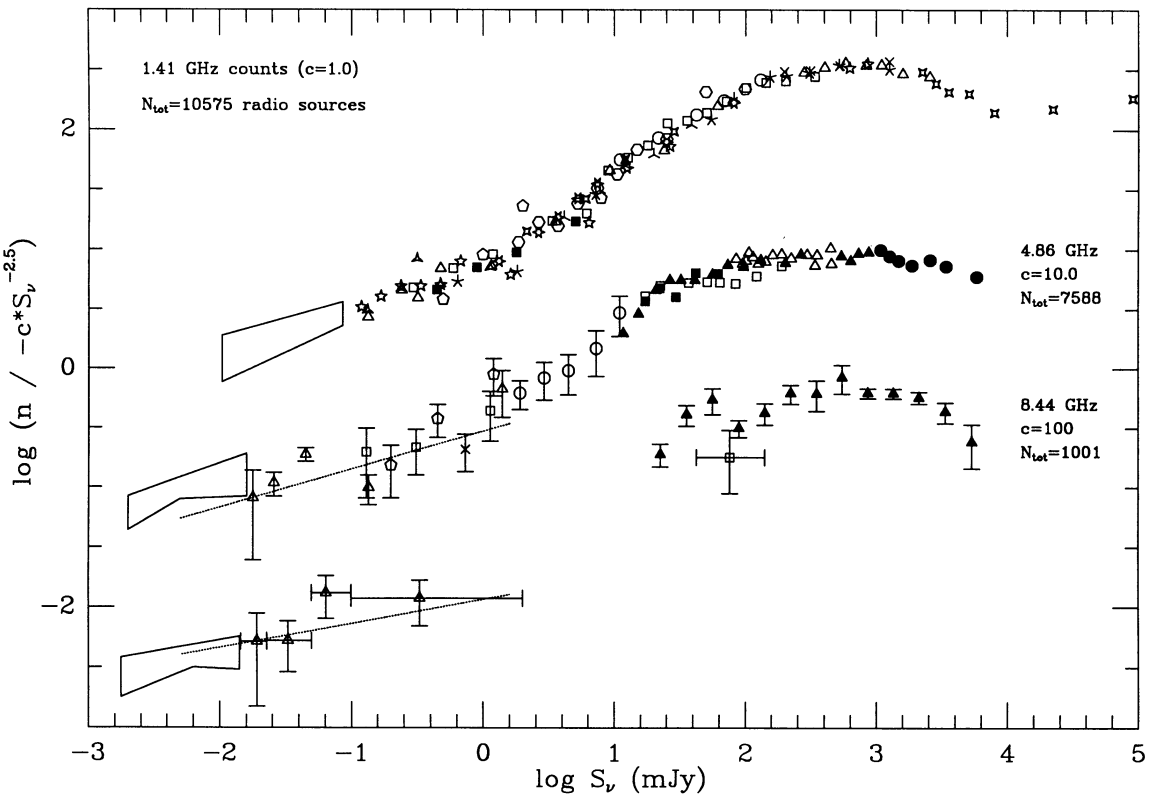

FIG. 3.—Differential source counts at 1.41, 4.86, and 8.44 GHz, *normalized* to a Euclidean count of $cS_\nu^{-2.5}$ (Jy^{-1} sr^{-1}). For clarity, the 4.86 GHz counts were scaled downward with $c = 10$, the 8.44 GHz counts with $c = 100$, while the 1.41 GHz were not shifted ($c = 1.0$). The various source samples are reviewed in the text. The counts at all three frequencies now cover a factor of 10^7 in S_ν. They all show the initial steep rise between $S_\nu \simeq 10$ and 1 Jy, the maximum excess plateau with respect to Euclidean between $S_\nu \simeq 1.0$ and $S_\nu \simeq 0.1$ Jy, and continuous convergence between $S_\nu \simeq 100$ and $S_\nu \simeq 3$ mJy. At all three frequencies, the counts show an upturn between $S_\nu \simeq 3$ and $S_\nu \simeq 3000$ μJy with a similar slope ($\gamma \simeq 2.2 \pm 0.2$).

resolution bias. Column (9) gives the number of sources expected for a differential Euclidean count $dN_E/dS_{8.44} = -1.0S^{-2.5}$ (Jy^{-1} sr^{-1}). Column (10) gives the resulting normalized differential 8.44 GHz source count: column (8)/column (9). The statistical error in the count is equal to $n_S^{1/2}/n_{Eucl}$.

The resulting 8.44 GHz counts are plotted in Figure 3. We also included the high-frequency, bright source count obtained by Aizu et al. (1987) at 10.0 GHz (see also Tabara et al. 1984). We rescaled their 10 GHz counts for the small frequency difference, using the median spectral index as a function of $S_{4.9}$ as discussed in § 6.3 (accounting for the fact that for *large* 8.44 GHz flux densities, the median spectral index may be ~ 0.1 flatter than implied by the high-frequency α_{med} versus $S_{4.9}$ relationship). Figure 3 also shows an estimate of the 8.44 GHz count from Seielstad's (1983) 10.7 GHz survey. He only detected two sources in 0.00158 sr down to $S_{10} \gtrsim 50$ mJy, which is statistically consistent with Aizu et al. (1987), who found 101 sources at 10 GHz in 0.0691 sr effectively down to $S_{10} \gtrsim 30$ mJy. The resulting single 10.7 GHz data point from Seielstad (1983) was also transformed to 8.44 GHz using the α_{med} versus $S_{4.9}$ relationship described in § 6.3.

The box in Figure 3 at the faint end of the 8.44 GHz counts indicates the limits to the source density in the range 1.5 μJy $\lesssim S_{8.44} \lesssim 14.5$ μJy from a statistical analysis of noise fluctuations in our 10″ FWHM image below the 14.5 μJy detection limit (see Fomalont et al. 1993, 1991a). For this we assumed that all of the excess fluctuations in the image—beyond that expected from receiver and instrumental errors—was produced by weak radio sources with a median angular size of $2\farcs6 \pm 1\farcs4$. As explained in § 5.1, the rather uncertain value of Θ_{med} does not affect the amplitude of the fluctuation boxes very much, since the 10″ beam size is much larger than Θ_{med}, so that the "resolution correction" to even the faint unresolved sources is small (if all of the sources below 2 σ were unresolved at 10″, their number density in the relevant flux density range would only decrease by about 20%). The fluctuation constraints to the source counts are best determined at a level of about 2 σ. The fluctuation count is not as well determined at lower flux density levels, because these faint sources start blending, and at higher flux densities, because the number of brighter sources is smaller. This is reflected in the shape of the boxes.

A maximum-likelihood fit to a power-law distribution of the observed source flux densities between 14.5 and ~ 1500 μJy in the combined Lynx and Cepheus fields is

$$N(>S) = (0.157 \pm 0.025)(S/40)^{-1.3\pm0.2}\,\mu\mathrm{Jy}^{-1}\ \mathrm{arcmin}^{-2}$$
$$= (3.57 \pm 0.57)S^{-1.3\pm0.2}\,\mathrm{Jy}^{-1}\ \mathrm{sr}^{-1}, \quad (2)$$

where $N(>S)$ is a convenient *integral* representation of the counts, indicating the number of sources with flux density greater than $S_{8.44}$ in the specified units. This fit has its flux density normalized to the weighted mean sample flux density ($S_{8.44} = 40$ μJy), where the slope and multiplicative constants of the power law are uncoupled in their error distributions.

The corresponding *differential* count, normalized to Euclidean, is

$$dN(S)/dN_E(S) = (-4.63 \pm 0.74)(S/\mathrm{Jy})^{+0.2\pm0.2}$$
$$= (-0.29 \pm 0.05)(S/\mu\mathrm{Jy})^{+0.2\pm0.2} \quad (3)$$

This count is valid in the range 14.5 μJy $< S_{8.44} \lesssim 1500$ μJy and corresponds to about 60% of the 4.86 GHz source density observed at the equivalent flux density of $S_{8.44} \sim 40$ μJy (Fomalont et al. 1991a). The expected fraction is $\langle\gamma\rangle\langle\alpha\rangle \simeq 2.3 \times 0.35 \simeq 80\%$, with $\langle\alpha\rangle$ from § 6.2. The count slopes at the two frequencies thus agree within the errors. The slope of the microjansky source count remains close to $\gamma \simeq 2.3$ down to 4 μJy when we include the image noise analysis of Fomalont et al. (1993), as shown by the fluctuation box in Figure 3.

5.3. *Comparison of the* 1.41, 4.86, *and* 8.44 GHz *Counts*

Figure 3 also gives the normalized differential 1.41 GHz source count as reviewed by Windhorst et al. (1990) and the normalized differential 4.86 GHz source count as reviewed by Kellermann & Wall (1987) for $S_{5.0} \gtrsim 10$ mJy and by Fomalont et al. (1991a) for $S_{4.9} \lesssim 10$ mJy. Where needed, the flux density scales of all 20–21 cm surveys were transformed to 1.410 GHz with the *low*-frequency median spectral index (α_{med}) versus flux density relation of Windhorst et al. (1990), and all $\sim$6 cm surveys to 4.860 GHz with the *high*-frequency α_{med} versus flux density relation of § 6.3. The abscissa in Figure 3 is log S_ν (in mJy), and the ordinate is the differential count divided by $S_\nu^{-2.5}$ (in $\mathrm{Jy}^{-2.5}\ \mathrm{sr}^{-2.5}$). To maintain clarity in Figure 3, the 4.86 GHz source counts are displaced downward by a factor of 10, and the 8.44 GHz counts by a factor of 100. The dotted lines are power-law best fits to the 4.86 and 8.44 GHz counts for $S_\nu \lesssim 2$ mJy.

At all three frequencies, the source counts now cover about a factor of 10^7 in S_ν (with a gap at 3.6 cm for 1 mJy $< S_{8.44} <$ 30 mJy). All three frequencies show the initial steep rise between $S_\nu \simeq 10$ and $S_\nu \simeq 1$ Jy (the 1.41 GHz counts actually cover enough area to also show the Euclidean plateau between 100 and 10 Jy which is dominated by nearby sources). All three frequencies show the maximum excess with respect to the Euclidean prediction between $S_\nu \simeq 1.0$ and $S_\nu \simeq 0.1$ Jy, and the subsequent continuous convergence between $S_\nu \simeq 100$ and $S_\nu \simeq 3$ mJy. The plateau of maximum excess appears widest at 4.86 GHz, because of the relative contribution of steep- and flat-spectrum sources as a function of flux density (see § 6.3). At 1.41 and 4.86 GHz, the slope of the count clearly changes below $S_\nu \simeq 3$ mJy. The 8.44 GHz count must also change slope near this flux density, but we cannot say where, since we lack data in the 3–30 mJy range. At all three frequencies, there is *no* significant change in slope between $S_\nu \sim 3$ and $S_\nu \sim 3000$ μJy (when including the fluctuation boxes). The average normalized differential count slope for the three frequencies in this range is $\gamma \simeq 2.2 \pm 0.2$. At all three frequencies, the amplitude of the normalized differential counts at 20 μJy is about 0.5%–2% of the source density expected from a Euclidean extrapolation of the strong sources at the jansky level. An upturn in the submillijansky source counts was first reported in surveys at 1.41 and 4.86 GHz (e.g., Windhorst 1984; Condon & Mitchell 1984; Windhorst et al. 1985; Donnelly et al. 1987; Fomalont et al. 1988, 1991a). This upturn is now seen at all three frequencies over nearly a factor of 10 in frequency and 1000 in flux density. This suggests that the same microjansky source population covers a fairly wide range of frequencies.

As explained in § 6.4, the bulk of the faint radio source population is likely at substantial redshifts ($z \gg 0.1$). The fact that the microjansky source counts sustain a nearly Euclidean slope over almost a factor of 10 in frequency and a factor of 1000 in flux density (Fig. 3) indicates that the weak radio source population—if it is indeed one population—likely has undergone cosmological evolution similar to that of giant elliptical radio galaxies and quasars, in that they were also more powerful and/or more frequently radio sources in the past. Only if the dominant population of microjansky sources were normal spiral or low-luminosity elliptical galaxies at $z < 0.1$ would evolution not be needed to explain the steep slope of the microjansky counts.

Note that an upturn was not seen in the 0.61 GHz counts of Windhorst et al. (1990), since these are not deep enough, or in the deeper 0.33 GHz counts of Oort et al. (1988) or Wieringa (1991), since below $\sim$0.5 GHz turnovers are seen in a significant fraction of the weak radio source spectra (Oort 1987). Oort suggested that his variable microjansky sources have low-frequency turnovers due to synchrotron self-absorption (SSA) at an average rest-frame frequency of $\lesssim$0.75 GHz. Because the median redshift of the (sub)millijansky population is of order 0.5–0.75 (see § 6.4), this turnover could be redshifted past the 0.61 GHz band, and thus generally be visible only at $\lesssim$0.33 GHz, explaining the general lack of upturn in the deepest 0.33 GHz counts. The alternative is that most of the microjansky sources are starburst galaxies with a nuclear starburst and free-free absorption below 0.5–1 GHz, but generally no central monster (e.g., Condon et al. 1991). Only higher resolution and deeper 8.44 GHz images can distinguish between these possibilities. It is also possible that both Oort's and Condon's model are correct, in that Condon's nuclear starburst model appears to be the dominant physical process but only at low redshifts (Condon et al. 1991 only sample nearby objects), while Oort's starburst + active galactic nucleus (AGN) model may be operating primarily in the distant samples ($z \gg 0.1$). This would naturally follow from the cosmological evolution of weak AGNs, which at low radio powers only cuts on at $z \gtrsim 0.3$ (Windhorst 1984).

5.4. *Limits to the Nanojansky Source Counts at High Frequencies*

Extending the count to nanojansky flux density levels will be difficult, for the following reasons. At 4.86 and 8.44 GHz flux levels of 1–2 μJy, the density of radio sources is about 15 arcmin^{-2} (eq. [2]). This density corresponds to an average separation between radio sources of only 15″, which is $\sim$6 times their median angular size (see § 5.1). Our survey is thus not yet confusion-limited, but weaker sources will begin to merge, and counting them individually will become increasingly difficult. Statistical analysis methods, combined with optical identifications of higher resolution VLA sources on deep CCD frames, will be required to deblend sources in deeper confusion-limited surveys (see also Fomalont et al. 1991a).

However, at nanojansky levels the differential counts must flatten at all frequencies with a slope $\gamma \leq 2$, or the integrated flux density of the emission from weak sources would diverge, and distort the low-frequency "thermal" spectrum of the 2.74 K cosmic background radiation. The most relevant direct measurements of the sky brightness near or below our 8.44 GHz observations are 2.61 $\pm$ 0.06 K at 3.0 cm (Kogut et al. 1988), 2.64 $\pm$ 0.06 K at 4.0 cm (Levin et al. 1992), 2.70 $\pm$ 0.07 K at 6.3

cm (Mandolesi et al. 1986), 2.59 ± 0.13 K at 8.1 cm (De Amici et al. 1988), and 3.0 ± 1.2 K at 50 cm (Sironi et al. 1990). Using a value of 2.74 K for the CBR background, these results suggest that a radio source background of 0.01 K at 3.6 cm, corresponding to about 0.04 K at 6.3 cm, 0.07 K at 8.1 cm, and 5 K at 50 cm (very uncertain extrapolation using $\langle\alpha\rangle = 0.35$), could still be consistent with these other measurements.

If the 8.44 GHz count in equation (2) continues down to 1 μJy with the same slope $\gamma = 2.3$, the corresponding sky brightness temperature from these sources would be 3×10^{-4} K. Continuation of the same slope down to 20 nanojanskys would produce a sky brightness temperature of 0.01 K from discrete 8.44 GHz sources alone. (When γ decreases below 2, the integrated flux density of weak sources below the break in slope becomes negligible.) Hence, we conclude that the apparent thermal spectrum of the isotropic sky background between 3 and 50 cm wavelengths implies an upper limit on sky brightness of roughly 0.01 K from weak sources at 8.44 GHz. Thus, the slope of the count must turn over permanently around 20 nanojanskys to avoid this sky brightness temperature limit. Firmer constraints to the nanojansky counts are given in § 6.4.

6. SPECTRA OF WEAK 8.44 GHz SOURCES

In this section we describe the radio spectral properties of the weak 8.44 GHz population in order to constrain the nature of the emission mechanism in these weak radio galaxies. Because the 8.44 GHz primary beam is very small, the complete sample only contains 20 sources. Moreover, sources in the complete sample are close to the 8.44 GHz primary-beam center and are sometimes too faint to be detected in the lower frequency deep surveys. Considerable data are also available at lower frequencies for 8.44 GHz sources with $S_{8.44} \geq 4.5\ \sigma$ but at $\geq 8'$ from the field center. Since these are probably real sources, but *not* in our complete 8.44 GHz sample (see § 4.2), we will consider them separately. It turns out that they generally confirm the spectral index trends seen in the smaller complete sample.

6.1. *Data from Lower Frequency Surveys*

Here we summarize all available spectral information on our weak 8.44 GHz sources from previous deep surveys in the same fields, mostly at frequencies lower than 8.44 GHz.

The Lynx field was imaged by Oort (1987) and Oort et al. (1988) at 327 MHz down to 0.9 mJy, and by Wieringa (1991) down to 0.5 mJy; by Windhorst (1984) and Windhorst & Oppe (1993) at 608.5 MHz down to 0.42 mJy; by Windhorst et al. (1984a) and Oort & Windhorst (1985) at 1412 MHz down to 0.12 mJy and 0.062 mJy, respectively; by Windhorst et al. (1985) at 1461.775 MHz down to 0.0285 mJy; by Donnelly et al. (1987) at 4.86 GHz down to 0.015–0.021 mJy; and by Hogan & Partridge (1989) at 14.940 GHz down to 0.028 mJy. The latter 2 cm VLA survey was the only one at a higher frequency than ours, and the only one that did not yield any detections of our 8.44 GHz sources.

The Cepheus field was previously imaged by Partridge, Hilldrup, & Ratner (1986) and Martin & Partridge (1988) at 4.86 GHz down to 0.011–0.015 mJy, and by Martin, Partridge, & Rood (1980) at 2.695 GHz down to 3 mJy and at 8.085 GHz down to 2 mJy. Source flux densities from the earlier 2.695 and 8.065 fluctuation surveys can be found in Partridge et al. (1986).

The published flux densities in these complete lower frequency samples (typically down to 4.5–5.0 σ) were used to determine the spectra for our 8.44 GHz sources. The spectral index determination is not affected by resolution effects for sources smaller than 15″ (which includes most of the sources), because the elliptical Gaussian source-fitting algorithm used in all surveys nearly reconstructs the total image flux density, even for significantly extended sources (see § 4.3.1).

Furthermore, we searched through all these lower frequency source lists (published or private communications) for additional sources in the 3.0–5.0 σ range that are nearly coincident with our 8.44 GHz sources (within 20″ or 1.5 times the typical HPBW). These sources are *not* in the *complete* low-frequency samples but may be used to determine *additional* source spectra in our complete 8.44 GHz sample, albeit with somewhat larger errors. For 8.44 GHz sources not detected in the lower frequency surveys, we determined 3 σ flux density upper limits using the known rms noise in the lower frequency images (as a function of distance to the respective field centers).

6.2. *Individual* 8.44 GHz *Source Spectra*

Radio spectra for sources in Table 1 are shown in Figures 4*a* and 4*b*. All flux densities are on the Baars et al. (1977) scale. Filled symbols with error bars indicate the actual measurements; open symbols without error bars indicate 3.0 σ upper limits. Dotted lines connect the measurements for each source. They are not intended to represent the best fits to the spectra, just to help distinguish between sources. The 8.44 GHz source name is listed to the right of the appropriate dotted line. Upper limits were not plotted in Figures 4*a* and 4*b* if an 8.44 GHz source was too faint to be detectable in the lower frequency surveys (because the resulting upper limits would be uninteresting).

Figure 4*a* shows the 20 sources in the complete catalog (all detected in the primary-beam main lobe with $S_p \geq 4.5\ \sigma$). Sixteen of these were detected in previous deep 4.86 or 1.41 GHz surveys, and some were detected at 0.61 or 0.33 GHz as well. Figure 4*b* shows the spectra for additional sources in the incomplete sample. Sources in the latter sample with $S_{8.44} \lesssim 0.3$ mJy occur in the primary-beam main lobe as well, but have $4.0\ \sigma \lesssim S_p \lesssim 4.5\ \sigma$, while the ones with $S_{8.44} \gtrsim 0.3$ mJy all occur by definition close to the peak of the first sidelobe. Figure 4*b* shows that almost all sources in this additional sample were detected at (usually two) lower frequencies, so that they are *not* spurious. The brightest two sources in Figure 4*b* have 8.44 GHz flux densities as expected from a straight extrapolation of the lower frequency data, supporting the discussion of § 4.2 that the peak of the first sidelobe is about 15 ± 2 dB. Some of the spectra that are very strongly inverted in Figure 4*b* ($\alpha \lesssim -1.5$ for $S_\nu \propto \nu^{-\alpha}$) may occur because these sources are close to the first or second null, where the 8.44 GHz attenuation is highly uncertain. However, about 10%–15% of the sources in the complete sample also have inverted spectra ($-2.0 \lesssim \alpha \leq 0.0$), which is believed to be a real effect (see below).

If a source was detected at the same frequency in several independent surveys at different epochs, all measurements were plotted, so that source variability at a given frequency can be judged from Figures 4*a* and 4*b*. This occurred primarily at 1412–1462 MHz, where two out of 11 sources (or two out of six

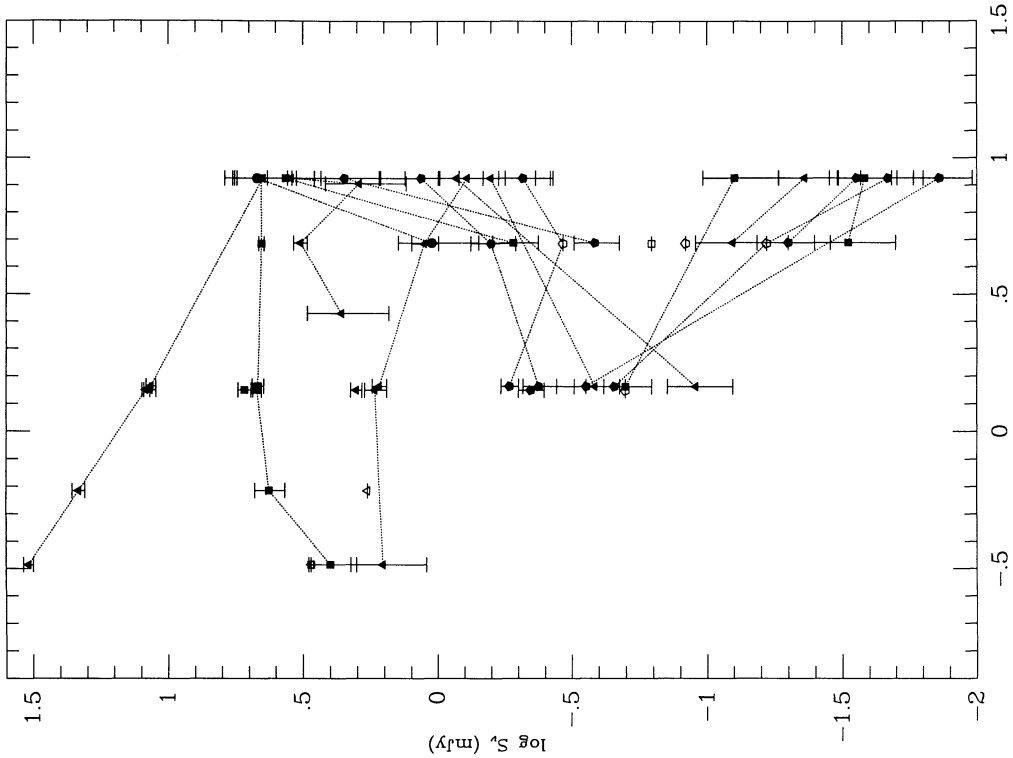

FIG. 4b

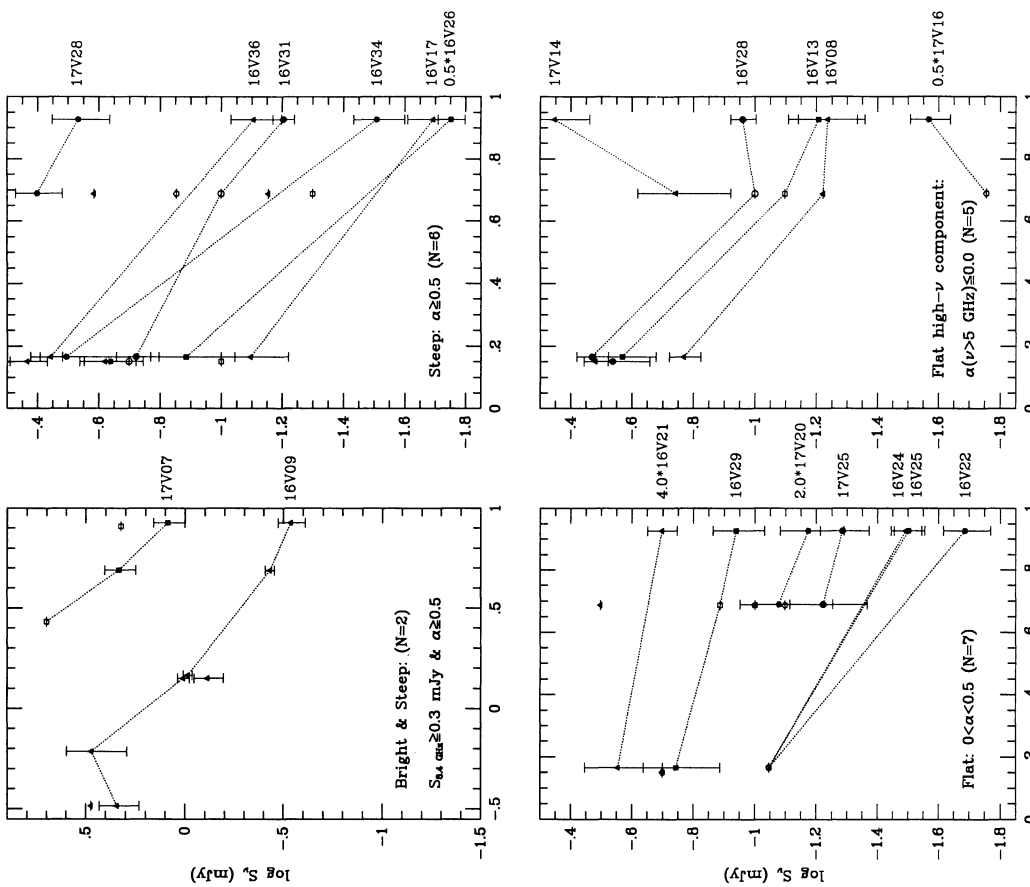

FIG. 4a

FIG. 4.—Three to five point radio spectra for weak radio sources selected at 8.44 GHz. (*a*) for the complete sample of 20 sources with $S_p \geq 4.5\,\sigma$ and radius less than 4'.59 (8% attenuation contour) and (*b*) for additional 8.44 GHz sources *not* in the complete sample. Points without error bars indicate 3 σ upper limits. The dotted lines are *not* best fits to the data, and serve only to distinguish among sources. The upper panels of (*a*) show the steep-spectrum sources, the lower panels show flat- and some inverted-spectrum sources.

in the complete 8.44 GHz sample) show significant ($\gtrsim 3\ \sigma$) variability on time scales of years (source 16V29 varied by more than 0.5 dex, so that its other epoch measurement is not visible in Fig. 4*a*). Oort & Windhorst (1985) found $\gtrsim 12\%$ variable sources among a larger 1.41 GHz sample in the Lynx field down to 0.3 mJy. The fraction of microjansky high-frequency sources that are variable on time scales of years is thus not negligible.

The complete sample in Figure 4*a* shows two *bright* sources in the upper left-hand panel. One has spectral information down to 0.33 GHz, and a possible spectral downturn below 0.6 GHz. The eight sources in the upper two panels all have steep high-frequency spectra (with $\alpha_{8.4}^{4.9}$, or, if not available, $\alpha_{8.4}^{1.4} > 0.5$) with mean value $\langle\alpha\rangle = 0.87 \pm 0.26$ ($1\ \sigma$ about the mean). Their median angular size is $\Theta_{\rm med} \simeq 3''$–$4''$. In the light of the discussion of § 6.4, these sources are presumably synchrotron disks in distant galaxies with possibly high-frequency spectral steepening due to synchrotron losses, and some AGN contribution (one of the steep-spectrum sources is $\gtrsim 3\ \sigma$ variable, and the low-frequency turnover of the brightest source indicates a self-absorbed radio core). The 12 sources in the lower two panels of Figure 4*a* have flat high-frequency spectra (with $\alpha_{8.4}^{4.9}$ or $\alpha_{8.4}^{1.4} \leq 0.5$ given their errors), while possibly three to five sources have additional high-frequency components (shown in the lower right-hand panel). These 12 sources have $\langle\alpha\rangle = 0.1 \pm 0.5$ (σ) and $\Theta_{\rm med} \simeq 5'' \pm 1''$, extending to $17''$ in size. At least two of these 12 sources have a flat high-frequency spectral index $\alpha \simeq 0$, consistent with a optically thin thermal bremsstrahlung component. Two others have strongly inverted high-frequency spectral components ($\alpha \lesssim -1.5$), which could be the optically thick part of a thermal bremsstrahlung component that cuts on at very high frequencies. These sources with high-frequency components are quite large as well ($\Theta \simeq 5''$–$13''$), while one of them is $\gtrsim 4\ \sigma$ variable. They are probably a combination of a steep-spectrum synchrotron disk (radiating primarily at low frequencies) plus a dominant flat or inverted spectral component, which could be either free-free emission from a starburst, or synchrotron emission from a weak AGN (in case of the variable source), or both.

The entire complete sample has a mean and median high-frequency spectral index of about 0.5 ± 0.2 (m.e.). The fraction of flat-spectrum sources—usually defined as $f(\alpha < 0.5)$—is thus $\simeq 50\%$. However, this fraction is affected by a few upper limits on α in the flat-spectrum panels. Donnelly et al. (1987) discuss the bias against the flattest spectrum sources at the faintest flux densities when selecting sources at the higher frequency. Using their correction for this bias, we find that the median spectral index drops to $\alpha_{\rm med} \simeq 0.35 \pm 0.15$, consistent with the values $\alpha_{\rm med} \simeq 0.4$ found for $S_{4.9} \gtrsim 100\ \mu$Jy by Donnelly et al. (1987), and $\alpha_{\rm med} \simeq 0.2$–$0.3$ found for $S_{4.9} \gtrsim 15\ \mu$Jy by Fomalont et al. (1991a). If indeed $\alpha_{\rm med} = 0.35 \pm 0.15$ for the complete 8.44 GHz sample, the true fraction of flat-spectrum sources, $f(\alpha < 0.5)$, must be $\gtrsim 50\%$, consistent with the 55% fraction found (at 4.86 GHz) by Donnelly et al. (1987) and the 60% fraction of Fomalont et al. (1991a).

In conclusion, the microjansky radio source population selected both at 8.44 GHz and at 4.86 GHz is primarily of the flat-spectrum class ($\alpha < 0.5$), as it is at brighter high-frequency flux density levels. At the expected median redshift of the microjansky sample ($z_{\rm med} \sim 0.5$–0.75; see § 6.4), these sources thus still emit significant flux at rest-frame frequencies in the range 13–15 GHz. This may have consequences for the *COBE* DMR experiment, as discussed in § 6.5.

6.3. *The Median Spectral Index versus High- and Low-Frequency Flux Density*

In this section, we briefly compare the flux density–dependent spectral index distribution of high-frequency surveys (ours at 8.44 GHz and the 4.86 GHz samples of Fomalont et al. 1991a and Donnelly et al. 1987) to those at low frequencies (as reviewed by Windhorst et al. 1990). The median spectral index versus flux density relation contains information about the redshift and/or luminosity dependency of the typical spectral index of the radio source population (Gopal-Krishna 1988).

Figure 5*a* shows the median spectral index measured in radio surveys selected at *low* frequencies (0.41–0.61 GHz), as discussed by Windhorst et al. (1990). Figure 5*b* shows the relation between median spectral index and flux density for samples selected at *high* frequencies. Because deep surveys at 8.44 GHz are scarce as yet, the highest available selection frequency with reasonable statistics is 4.86 GHz. The median spectral indices, $\alpha_{\rm med}$, were taken from the literature summary of Fomalont et al. (1991a), which covers microjansky to jansky levels. We also plotted our 8.44 GHz value of $\alpha_{\rm med} = 0.35 \pm 0.15$ in Figure 5*b*, after transforming our median sample flux to 4.86 GHz, using this $\alpha_{\rm med}$ value. Figures 5*a* and 5*b* are plotted above each other in such a way that a vertical line intersects the flux densities of the same radio sources at the different frequencies. This roughly accounts for the different flux density scales between the two frequencies, as determined by this relationship.

The general dependences of the median spectral index $\alpha_{\rm med}$ on flux density for the high- and low-frequency samples are similar. The dotted lines in Figure 5 are third-order weighted least-squares fits to the (logarithmic) data that illustrate the similarity between Figures 3 and 5. At the jansky level, the large fraction of flat-spectrum luminous quasars produces the initial low value of $\alpha_{\rm med}$, especially at high frequencies (where quasars dominate). The median spectral index reaches maximum steepness in the $S_\nu = 0.1$–1 Jy range, which is caused by the predominance of high-redshift luminous radio galaxies which have steeper spectral indices, and also cause the maximum excess in the counts with respect to Euclidean (Fig. 3). Below these flux densities, flat-spectrum powerful quasars become more rare, because their redshift would be greater than 3.5–4.0 (beyond which their space density declines rapidly).

Figure 5 shows that the median spectral index for the *low*-frequency sample decreases to $\lesssim 0.7$ below 3 mJy, while for the *high*-frequency sample the median spectral index decreases to ~ 0.4 below 1 mJy. The 4.86 GHz spectral index remains constant over almost a factor of 100 in flux density down to the faintest levels observed to date. As Fomalont et al. (1991a) point out, this is the largest range of flux density in which essentially no change in the spectral population occurs. Since the slope of the source count (§ 5.3) is also virtually constant in this flux density range, the corresponding mix of radio sources is apparently similar throughout the entire 15–1000 μJy flux density range at 4.86 and 8.44 GHz.

Using the relations of Figures 5*a* and 5*b*, the microjansky counts can be transformed between 1.41, 4.86, and 8.44 GHz—similar to the transformation between 0.61 and 1.41 GHz of Windhorst et al. (1990) at mJy levels—but only once the precise shape of the microjansky spectral index distribution is known at high frequencies. This will be addressed in a future paper when better statistics are available. From the current data, we conclude that the typical radio source spectral index

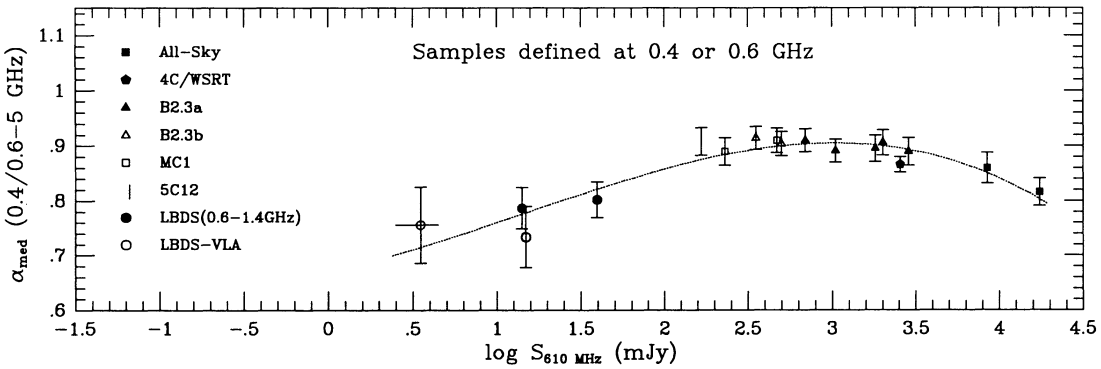

FIG. 5a

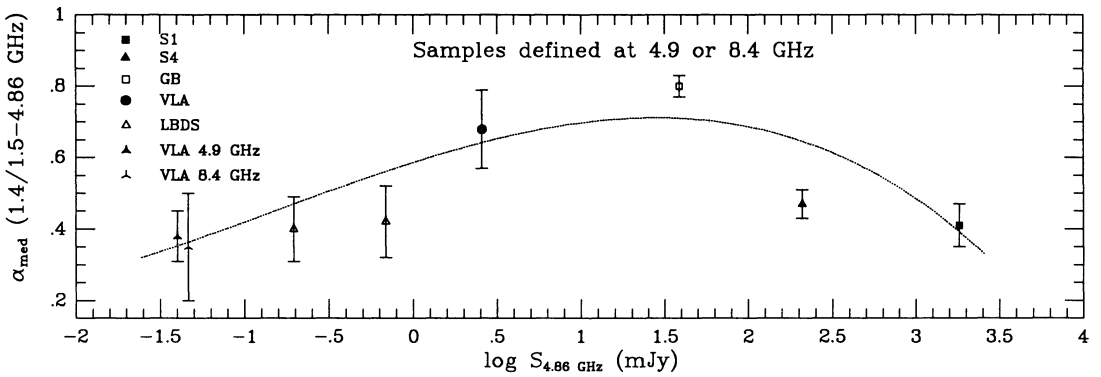

FIG. 5b

FIG. 5.—(*a*) Median spectral index: *low-frequency* flux density relation. The values of α_{med} were measured between 0.41 (or 0.61) GHz and 4.86 (or 5.0) GHz, and are plotted against 0.61 GHz flux density. (*b*) Median spectral index: *high-frequency* flux density relation. The values of α_{med} were measured between 1.41 (or 1.5) GHz and 4.86 GHz, and are plotted against 4.86 GHz flux density. The dotted lines are third-order weighted least-squares fits to the logarithmic data. Note the similarity of the source counts (Fig. 3) and the run of α_{med} with S_ν.

continues to flatten toward submillijansky flux density levels at both high and low frequencies.

6.4. *Constraints to the Nature and Evolution of Microjansky Radio Sources*

Deep optical CCD data are currently lacking for the LBDS field Lynx.2. We plan to present such data in a future paper. Here we discuss the currently available constraints to the nature and possible cosmological evolution of microjansky radio sources.

6.4.1. *Constraints from the Counts*

Below a few millijanskys, faint blue galaxies dominate the radio source population down to 50 μJy at 1.41 GHz (Windhorst et al. 1985, 1990; Oort 1987) and down to 15 μJy at 4.86 GHz (Fomalont et al. 1991a). The majority of these faint blue objects are believed to be star-forming galaxies at intermediate to high redshifts (Windhorst et al. 1987, 1990, 1991; Thuan & Condon 1987). Luminous giant elliptical radio galaxies with double-lobed sources, quasars, and radio stars comprise less than 30%–40% of the submillijansky identifications (Windhorst et al. 1985). Because the slope (§ 5.3; Fig. 3) and the average spectral index (§ 6.3; Figs. 5*a* and 5*b*) of the source counts remain constant in the flux density range $S_{4.9} \sim 15$ μJy–3 mJy *and* in the frequency range 1.41–8.44 GHz, and because more than about two-thirds of the optical identifications in the weak 1.41 and 4.86 GHz samples are blue galaxies, we expect that these objects also dominate the 8.44 GHz population on the 0.02–1 mJy range.

The optical magnitude distributions of faint radio sources span the range 18 mag $\lesssim V \lesssim$ 28 mag with a median $V \simeq$ 22–22.5 mag for $S_{1.4} \gtrsim 1$ mJy (Windhorst et al. 1987) and median $V \simeq 23.5$ mag for $S_{4.9} \gtrsim 15$ μJy (Fomalont et al. 1991a; Kristian, Windhorst, & Fomalont 1993). The median V flux thus possibly decreases somewhat with radio flux density. Magnitude-redshift diagrams are available for faint radio galaxies down to $S_{1.4} \gtrsim 80$ μJy (Windhorst et al. 1990) and down to $S_{1.4} \gtrsim 0.6$ mJy (Kron et al. 1985). At their median V-magnitude $\simeq$23 mag, the measured median redshift of radio galaxies with $S_{1.4} \gtrsim 0.08$ mJy is $z_{med} \gtrsim 0.4$–0.75 (Windhorst et al. 1990). Various models for the cosmological evolution of the faint source population predict similar median redshifts ($z_{med} \simeq 0.5$–0.85) for submillijansky sources (Windhorst 1984; Condon 1989). These models also show that z_{med} is only a weakly declining function of flux density below $S_\nu = 100$ mJy. Hence, we expect that radio sources with $S_\nu \gtrsim 10$ μJy have $z_{med} \simeq 0.5$–0.75.

We note in this context two important properties of field galaxies. First, the slope of the microjansky source counts ($\gamma \simeq 2.3 \pm 0.2$; § 5.2) is only marginally steeper than the slope of the (differential) *field* galaxy counts for $V \lesssim 27$ mag, or $B_J \lesssim 27.5$ mag. In the B_J filter, the slope of the blue galaxy counts follows from $dN/dm \propto m^{0.45 \pm 0.03}$ (Neuschaefer, Wind-

horst, & Dressler 1991; Neuschaefer 1992), which translates to $\gamma \simeq 2.13 \pm 0.07$ in regular flux density units. Second, at $V \simeq 23$ mag, field galaxies have a median redshift $z_{med} \simeq 0.4$ (Colless et al. 1990; Lilly, Cowie, & Gardner 1991), illustrating that their spectral evolution must have been mild since $z \simeq 1$ (e.g., Koo 1990). The slightly steeper slope of the microjansky radio source counts thus suggests that faint radio galaxies with $V \simeq 23$ mag may only have a slightly larger median redshift than that of field galaxies at $V \simeq 23$ ($z_{med} \gtrsim 0.4$), consistent with the value $z_{med} \simeq 0.5$–0.75 suggested above. If their median redshift is indeed this large, the steep slope of the microjansky source count suggests that these objects probably underwent cosmological evolution at a rate somewhat faster than the mild (spectral + luminosity) evolution of field galaxies, but not as fast as that of giant ellipticals and quasars, whose count has a much steeper initial slope (for $S_\nu \gtrsim 0.5$ Jy). A more quantitative statement will have to await distance measurements of sources at the microjansky level. In a future paper we will therefore present optical identifications on deep CCD mosaics in Lynx and Cepheus, and further constrain their nature and redshifts through spectroscopy (for $V \lesssim 23.5$ mag) and multiband optical colors (for 23.5 mag $\lesssim V \lesssim 28$ mag; see also § 6.4.3).

6.4.2. *Did the Microjansky Population Evolve?*

Local objects ($z \lesssim 0.1$) could in principle mimic the observed microjansky count slope without cosmological evolution, and possibly also their observed spectral and angular size properties. However, the microjansky radio galaxies cannot be a local ($z \lesssim 0.1$) unevolving population of low-power radio galaxies, because their implied absolute magnitudes would be 5–6 mag fainter than the values thus far observed for the 175 faint radio galaxies with measured spectroscopic redshifts (which have $M_V \simeq M_J \simeq -21.5$ mag for $H_0 = 50$ km s^{-1} Mpc^{-1}, close to the M^* value of field galaxies; Windhorst et al. 1990). Any local population would have to come up very suddenly below $S_\nu \simeq 0.1$ mJy (most of the redshifts so far have been measured for $S_\nu \gtrsim 0.08$ mJy), inconsistent with the continuity in slope and spectral properties (§§ 5.3 and 6.2). If most microjansky radio galaxies really had $z_{med} \lesssim 0.1$, they would have to be local dwarf galaxies, but such objects are not found in local radio surveys at the implied relatively high radio powers ($P_{1.4} \simeq 10^{21}$–10^{22} W Hz^{-1} for $H_0 = 50$; Pfleiderer 1977; Hummel 1981a, b; see also Windhorst 1984, 1986).

6.4.3. *Can All Their Redshifts Be Measured?*

The magnitude-redshift diagrams for sources with $S_\nu \gtrsim 0.1$–1 mJy show that their optical luminosities are at most ~ 1 mag lower than those of the "standard candle" giant ellipticals which dominate for $S_{1.4} \gtrsim 3$–5 mJy (Kron et al. 1985). If their median redshift is indeed ~ 0.5–0.75, a considerable fraction of objects is still expected for $1 \lesssim z \lesssim 2$. The optically faintest microjansky radio galaxies found at 4.86 GHz have 26 mag $\lesssim V \lesssim 28$ mag (Fomalont et al. 1991a). If these objects are indeed at $z \simeq 2$, the optical filter bands sample their rest-frame mid-UV continuum. Spectral evolution models consistent with the observed color-redshift and magnitude-redshift diagrams suggest that radio galaxies with $V \gtrsim 26$ mag are at least at $z \gtrsim 0.75$, and probably at $z \gtrsim 1$ (Windhorst et al. 1990), so that the V-band samples at least their rest-frame mid-UV. To produce galaxies as faint as 26 mag $\lesssim V \lesssim 28$ mag, their star formation rate must be rather low, as deduced from the range of rest-frame mid-UV spectra seen in nearby and distant radio galaxies (see Figs. 7 of Keel & Windhorst 1991 and Windhorst et al. 1991). Radio galaxies at $z \simeq 2$ with high star formation rate would show up with $V \simeq 22$–23 mag (Windhorst et al. 1991 and references therein). Hence, the star formation rate in the optically faintest microjansky radio galaxies cannot be as high as that in nearby luminous starburst galaxies seen by *IRAS*, or in the ultraluminous and 3 CR and 1 Jy radio galaxies recently discovered at $z \gtrsim 2$. Without high star formation rate, microjansky galaxies with $V \gtrsim 26$ mag will have a small Lyα equivalent width, below that of luminous starburst galaxies and closer to that of normal radio spirals. Since Lyα is likely the strongest emission line in weak radio galaxies (Keel & Windhorst 1991), it may well be impossible to measure their redshifts, even with the next generation of telescopes. Moreover, the sky becomes spectroscopically confusion-limited for $V \gtrsim 26$ mag (Neuschaefer et al. 1991), so that their redshifts may not be measurable until 10 m class telescopes are available in space where the sky background is a few magnitudes lower than on the ground (Windhorst et al. 1992).

6.4.4. *Constraints to the Nature of Microjansky Sources*

In § 5.1 we concluded that microjansky radio sources have angular sizes as large as at millijansky levels, and in § 6.3 we concluded that their spectral indices are somewhat flatter than at millijansky levels. At the expected median redshift of the microjansky sample ($\simeq 0.5$–0.75), the median angular size of $\Theta_{med} = 2\farcs6 \pm 1\farcs4$ (§ 5.1) corresponds to linear sizes in the range ~ 5–40 kpc (for the likely range of $H_0 = 50$–100 km s^{-1} Mpc^{-1}, $q_0 = 0$–0.5). This is bigger than that expected from nuclear starbursts or AGNs alone. The evidence presented in § 6.2 suggests that the radio emission in microjansky 8.44 GHz sources is a combination of steep-spectrum synchrotron components in galactic disks at intermediate to high redshifts, plus thermal bremsstrahlung from large-scale star formation. About 10%–20% of the objects may also have an embedded nuclear starburst (free-free emission is seen in the nuclear starbursts of nearby galaxies; Condon et al. 1991), or weak flat-spectrum radio cores (whose power is expected to increase with redshift due to the cosmological evolution of AGNs. Donnelly et al. (1987) and Oort (1987) suggested this nonthermal disk + AGN mechanism for their 4.86 GHz sources down to 80 μJy. To further disentangle the relative importance of these possible mechanisms as a function of redshift, higher resolution and sensitivity 8.44 GHz observations are needed for our sample.

6.4.5. *Tighter Constraints to the Nanojansky Source Counts*

The continuity of *both* the median spectral index *and* the slope of the microjansky source counts suggests that microjansky radio galaxies are less luminous, but similar to the starburst galaxies seen at brighter radio levels. The data of §§ 5 and 6.3 suggest that these objects are reasonably well mixed in their radio luminosity and space distribution. They may well form a continuous and decreasing sequence of star formation, such that the weaker radio galaxies have less star formation (or their optical identifications would be brighter than $V \simeq 23.5$–24 mag, regardless of their redshift). As a consequence, the counts below ~ 30 μJy would be completely dominated by ordinary spiral galaxies. This is another reason why the counts must turn over with a converging slope ($\gamma \leq 2$) below $S_\nu \lesssim 1$ μJy, because at $S_\nu \simeq 30$ nJy most spiral galaxies (with powers in excess of the break in their local radio luminosity function) would have been seen out to $z \sim 2.5$ (Windhorst 1984), so that the number of extragalactic objects that can form nuclear + disk radio sources would become exhausted below $S_\nu \simeq 30$ nJy (this assumes that irregular and dwarf galaxies do

not form such sources in a significant way, as discussed above). This argument leads to an even firmer flux density limit below which the source counts must permanently converge. Most μJy radio sources in the complete sample of Fomalont et al. (1991a) have been optically identified down to $V \lesssim 28$ mag. The field-galaxy density down to $V \simeq 28$ mag is $(1.5\text{–}3) \times 10^{+5}$ deg^{-2} (Tyson 1988; Lilly et al. 1991; Griffiths et al. 1992). The extrapolation of the observed microjansky 8.44 GHz counts with constant slope $\gamma \simeq 2.3$ (eq. [2]) would exceed the surface density of available field galaxies with $V \lesssim 28$ mag for $S_{8.44} \lesssim 300$ nJy, where the radio source density reaches $\sim 10^9$ sr^{-1}.

We conclude that—within the errors of the above estimates—the source counts must *forever turn over* with slope $\gamma \leq 2$ below $S_\nu \lesssim 100$ nJy (± 0.5 dex). Since a good fraction of the high-frequency microjansky radio emission may be due to large-scale nonthermal or free-free processes in galaxy disks at intermediate redshifts ($z_{\rm med} \gtrsim 0.5$), the $\Theta_{\rm med}$ value of nanojansky radio sources may similarly stabilize at a few arcseconds. If this is true, then nanojansky radio surveys will always be limited by natural confusion, no matter what the instrumental resolution is.

6.5. *Contributions of Weak Discrete* 8.44 GHz *Sources to the COBE/DMR Beam*

If we may extrapolate the 8.44 GHz source density to 31.5 GHz, we could estimate the weak discrete source contribution to the *COBE*/DMR experiment (Bennett et al. 1992; Kogut 1992; Smoot et al. 1990, 1991, 1992). Hence, we need to extrapolate the 8.44 GHz count over a factor of 3.7 in frequency. For this, we adopt the same mean spectral index ($\alpha = 0.35 \pm 0.15$) between 8.44 and 31.5 GHz as measured between 1.41 and 8.44 GHz (§ 6.3; the required spectral extrapolation extends to the right-hand edge of Fig. 4*b*). A 3 σ change of this spectral index by ± 0.45 (barely allowed by Fig. 4) would affect the estimates below by about 0.5 dex.

As noted in § 5.4, the differential counts must converge around or below 20 nJy with a slope $\gamma \leq 2$, or the contribution from 8.44 GHz sources would distort the thermal CBR spectrum at centimeter wavelengths. For reasons explained in §§ 5.3 and 6.4, we will assume that the cosmological evolution of the microjansky sources is similar to that of giant elliptical radio galaxies and quasars (see also Windhorst 1984; Condon 1984, 1989). The normalized differential source counts of the classical luminous gE radio galaxies and quasars—which constitute the majority at millijansky and jansky levels—show a plateau between 0.1 and 1 Jy (Fig. 3), below which the logarithmic slope decreases by about 0.4–0.6 in the converging part of the counts (Windhorst et al. 1985, 1990). If the microjansky population has a similar epoch-dependent radio luminosity function and redshift distribution, then their count must similarly converge at nanojansky levels after this plateau region. Since the counts have a relatively constant slope $\gamma = 2.2 \pm 0.2$ for $S_\nu \simeq 3\text{–}3000$ μJy and $\nu \geq 1$ GHz, we consider this to be the plateau region of the count for these low-luminosity sources, and suggest that the slope will similarly flatten by ~ 0.5 (to $\gamma \simeq 1.7 \pm 0.2$) below 1 μJy (in particular below 100 nJy; § 6.4.5).

The contribution to the sky brightness temperature of this count at 8.44 GHz is (110 ± 20) μJy arcmin^{-2}, or 0.5 mK. Using an average spectral index of 0.35 ± 0.15 (see § 6.2), we obtain 23 μK at 31.5 GHz, or about 12 Jy within the 7° (FWHM) *COBE*/DMR beam. An upper limit to the source contribution in the *COBE*/DMR beam can be estimated from the spectral index error and the source count error. The resulting 3 σ limit is 36 μK at 31.5 GHz. Half of the total discrete radio source background is produced by sources with a flux density less than 1 μJy at 31.5 MHz.

Fluctuations in the radio sky produced from the discrete source background are difficult to estimate. The problem can be separated into fluctuations caused by the occasional bright source—or groups of bright sources—and by large-scale (but low-amplitude) angular changes in the weak radio source background. On the average, the brightest source in the *COBE* field of view is about 0.5 Jy, corresponding to a brightness temperature of ~ 1 μK. Assuming that the effects of the brightest known sources in the sky can be removed, fluctuations from the remaining bright sources should be no more than 1–2 μK.

The faint high-frequency source contribution with brightness temperature of $\lesssim 1$ μK will consist of thousands of radio sources in the nanojansky to millijansky range. If these were randomly distributed in the 7° *COBE* beam, field-to-field fluctuations would be much less than 1 μK and thus would cancel out in this differential experiment. However, larger field-to-field fluctuations may nonetheless arise in the source counts on scales of degrees due to high-redshift superclustering (Windhorst 1986; Windhorst et al. 1990; Oort 1987; Neuschaefer et al. 1991). This is because of a combination of the following factors. First, recent redshift surveys show that faint field galaxies are primarily arranged in sheets or superstructures typically $\Delta z \simeq 0.04$ in redshift apart (Broadhurst et al. 1990). Second, the redshift distributions thus far measured—as well as the best available source count models—suggest that most weak radio sources are *not* necessarily at very large redshifts (typical values of the ($\sim 95\%$) model redshift cutoffs are $z_{\rm max} \simeq 1.5\text{–}2.5$; Windhorst 1984; Condon 1984, 1989). If the large-scale clustering properties of galaxies indeed has evolved little with cosmic time since $z \simeq 1\text{–}2$ (Neuschaefer et al. 1991; Neuschaefer 1992), then the number of independent galaxy sheets in a *COBE*/DMR field that contains most of the radio sources will not greatly exceed $\sim 2/0.04 \simeq 50$. If the radio luminosity function within a supercluster is constant at a given redshift, then the rms field-to-field fluctuations in the radio source density could be as large as $\sim 1/(50)^{1/2} \simeq 15\%$ of the weak source contribution. Some evidence for 15%–20% field-to-field fluctuations on scales of degrees may be derived from the extensive 1.41 GHz source counts in many small regions of sky (for a review see Windhorst et al. 1990). Their summary contains 10,575 faint 1.41 GHz sources in 24 deep survey fields down to 0.08 mJy. The *observed* rms variance in these counts is $\sim 30\%$ on degree scales, while that expected from $N^{1/2}$ statistics is only $\lesssim 20\%$. Windhorst et al. (1990) argue that the combined systematics of flux density scale and resolution correction in these surveys is $\lesssim 15\%$, so that there is room for an *intrinsic* variance of $\lesssim 15\%\text{–}20\%$ in the 1.41 GHz count on degree scales ($\simeq$ typical supercluster size at $z \simeq 1$).

The nonnegligible contribution from nanojansky to millijansky sources at 31.5 GHz, *and* the possible $\lesssim 15\%\text{–}20\%$ fluctuations in the radio source density on degree scales, may result in temperature variations between *COBE* fields. From the above 3 σ limit of 36 μK, the maximum fluctuations in source density of $\lesssim 20\%$ on $\sim 1°$ scale allowed by the 1.4 GHz source counts, and the *COBE*/DMR beam of $\sim 7°$, we estimate a 3 σ upper limit to systematic fluctuations between *COBE*/DMR beams of $\lesssim 36 \times 0.20/[\pi(7/2)^2]^{1/2} \lesssim 1.2$ μK. Franceschini et al. (1989) estimated the discrete source contribution by extrapolation of the 5 GHz counts (as of 1988) to 33 GHz, and

predict a temperature fluctuation from discrete sources at the 7° scale of the *COBE* beam of 1.3 μK (using their $\alpha = 0.4$ curve, consistent with our measured value of $\alpha_{med} = 0.35$). This is consistent with our 3 σ upper limit, which is based on deeper counts at higher frequencies, and different clustering arguments. Our 1.2 μK upper limit is a bit less than the contribution expected from moderately bright sources, smaller than other known systematics in the *COBE*/DMR beam (Kogut et al. 1992), and smaller in amplitude than the structures recently found by *COBE* on scales of 10° (Smoot et al. 1992). However, the signal expected from weak radio sources will eventually constitute a natural limit (at the $\Delta T/T \simeq 0.4 \times 10^{-6}$ level) to measurements of CBR fluctuations on degree scales, which cannot be overcome without mapping all high-frequency sources down to $\lesssim 1$ μJy over many square degrees.

7. CONCLUSIONS

We have made deep images with 10″ resolution at 8.44 GHz with microjansky sensitivity of two regions previously imaged at several lower frequencies. From these images we have done the following:

1. Compiled a catalog of 82 sources between 14 and ~ 1000 μJy.
2. Determined the source count from a complete sample of 20 radio sources with $S_{8.44} \geq 14.5$ μJy and radius $\leq 4'.59$ (the VLA 8% attenuation contour).
3. Measured the positions of the sources to 1″ accuracy and determined their angular sizes, or upper limits thereof.
4. Determined their spectral index using data from lower frequency deep surveys.

The major results that we obtained from this 8.44 GHz survey are as follows:

1. The differential microjansky source count fits a power-law distribution with slope $\gamma = 2.3 \pm 0.2$. This slope is roughly constant between 1.41 and 8.44 GHz *and* between $S_\nu \simeq 4$ and $S_\nu = 1000$ μJy.
2. Unless the majority of radio sources at microjansky levels are local ($z \ll 0.1$), their average luminosity and/or space density likely has evolved with cosmic epoch in order to sustain the steep and nearly Euclidean value of the slope ($\gamma \lesssim 2.5$) over such a large range in flux density.
3. The 8.44 GHz counts likely converge (with slope $\gamma \leq 2.0$) at the $\lesssim 1$ μJy level, if the evolutionary properties of these weak sources are similar to those of luminous gE radio galaxies and quasars. They most likely converge below $S_\nu \simeq 300$ nJy, or they would exceed the available field galaxy counts down to $V \simeq 28$ mag. However, the counts *must permanently* converge for $S_\nu \lesssim 20$ nJy, or their integrated sky brightness temperature would exceed the observed thermal CBR spectrum at centimeter wavelengths.
4. The median angular size of sources detected at 8.44 GHz at microjansky levels is $2''.6 \pm 1''.4$, and 40% of the sources are larger than 5″. This angular size is surprisingly large compared with that of somewhat brighter sources (0.1–1 mJy).
5. Faint radio sources previously studied at 1.41 or 4.86 GHz are mostly identified with faint blue galaxies with 18 mag $\lesssim V \lesssim 28$ mag and median $V \simeq 22$–23.5 mag. Spectroscopy at somewhat brighter radio levels shows that the median redshift at $V \simeq 23$ mag is 0.6–0.75. Since z_{med} is only a weak function of flux density or frequency, we expect that $z_{med} \simeq 0.5$–0.75 at 8.44 GHz. Hence, their median linear size is 5–40 kpc (for $H_0 = 50$–100 km s^{-1} Mpc^{-1}, $q_0 = 0.0$–0.5).
6. The median spectral index of sources detected at 8.44 GHz at microjansky levels is 0.35 ± 0.15. Very few sources show high-frequency spectral steepening associated with the aging of synchrotron electrons. Some sources show a rising spectrum at 8.44 GHz.
7. The peculiar combination of flat spectral index ($\alpha \lesssim 0.5$) and rather large linear size has several possible explanations. The radio emission may be produced by thermal bremsstrahlung from large-scale star formation in distant galactic disks, or the source may be composed of a steep-spectrum nonthermal disk component with a flat-spectrum nuclear component (either a nuclear starburst with free-free emission or an opaque AGN core).
8. Extrapolation of the 8.44 GHz source count to 31.5 GHz suggests that fluctuations in the sky brightness temperature among the *COBE* fields should be less than 1.2 μK, even assuming a maximum slope of the counts and maximum possible superclustering (with $\lesssim 15\%$–20% amplitude) of radio sources on degree scales (as deduced from faint galaxy surveys and deep radio source counts in many small regions of sky).

More complete optical data are needed to determine the nature of these weak sources. Are the faintest radio sources indeed sufficiently distant that cosmological evolution is required to explain the surprisingly steep slope of the normalized differential source counts? Are most microjansky galaxies primarily blue, and how are they related to starburst galaxies which dominate the source count at the millijansky level? Does the high-frequency radio emission come from galactic disks, or the galactic nucleus, or from isolated features in the galaxies (e.g., supernova remnants, spiral arms)? What are their counterparts, if any, within 20 Mpc of the Milky Way?

Additional radio observations are needed as well. The characteristics of the weak 8.44 GHz population are based on only 20 sources in the complete sample. This number must be increased in order to determine the statistical properties of the microjansky population with more certainty. Observations of higher resolution and sensitivity are needed to determine their radio structure, and decide what causes these weak high-frequency sources: flat-spectrum, extended emission from thermal bremsstrahlung in galactic disks, or a superposition of an opaque (self-absorbed) core and a nonthermal disk component.

We thank Peter Napier for giving us his recent VLA primary-beam measurements, the VLA staff for their continuous help, Craig Hogan for helpful discussions, and an anonymous referee for useful comments. R. A. W. was supported by NSF grant AST-88211016 and the Alfred P. Sloan Foundation. R. B. P. was supported in part by grant AST-8914988 from the National Science Foundation. J. D. L. acknowledges support from a fellowship through the NASA Graduate Student Research Program.

REFERENCES

Aizu, K., Inoue, M., Tabara, H., & Kato, T. 1987, in IAU Symp. 124, Observational Cosmology, ed. A. Hewitt, G. Burbidge, & L. Z. Fang (Dordrecht: Reidel), 565
Baars, J. W. M., Genzel, R., Pauliny-Toth, I. I. K., & Witzel, A. 1977, A&A, 61, 99
Bennett, C. L., et al. 1992, ApJ, 391, 466
Broadhurst, T. J., Ellis, R. S., Koo, D. C., & Szalay, A. S. 1990, Nature, 343, 726
Clark, B. G. 1980, A&A, 89, 377
Coleman, P. H., & Condon, J. J. 1985, AJ, 90, 1431
Colless, M. M., Ellis, R. S., Taylor, K., & Hook, R. N. 1990, MNRAS, 244, 408

Condon, J. J. 1984, ApJ, 287, 461
———. 1989, ApJ, 338, 13
Condon, J. J., Huang, Z.-P., Yin, Q. F., & Thuan, T. X. 1991, ApJ, 378, 65
Condon, J. J., & Mitchell, K. J. 1984, AJ, 89, 610
De Amici, G., Smoot, G. F., Aymon, J., Bersanelli, M., Kogut, A., Levin, S. M., & Witebsky, C. 1988, ApJ, 329, 556
Donnelly, R. H., Partridge, R. B., & Windhorst, R. A. 1987, ApJ, 321, 94
Fomalont, E. B., Kellermann, K. I., Anderson, M. C., Weistrop, D., Wall, J. V., Windhorst, R. A., & Kristian, J. A. 1988, AJ, 96, 1187
Fomalont, E. B., Kellermann, K. I., Wall, J. V., & Weistrop, D. 1984, Science, 225, 23
Fomalont, E. B., Lowenthal, J. D., Partridge, R. B., & Windhorst, R. A. 1991b, in AIP Conf. Proc., Vol. 222, After the First Three Minutes, ed. S. S. Holt, C. L. Bennett, & V. Trimble (New York: AIP), 140
Fomalont, E. B., Partridge, R. B., Lowenthal, J. A., & Windhorst, R. A. 1993, ApJ, 404, 8
Fomalont, E. B., Windhorst, R. A., Kristian, J. A., & Kellermann, K. I. 1991a, AJ, 102, 1258
Franceschini, A., Toffolatti, L., Danese, L., & De Zotti, G. 1989, ApJ, 344, 35
Gopal-Krishna. 1988, A&A, 192, 37
Griffiths, R. E., et al. 1992, in ST-ECF/STScI Workshop on Science with the *Hubble Space Telescope*, ed. P. Benvenuti (Munich: ESO), in press
Hogan, C. J., & Partridge, R. B. 1989, ApJ, 341, L29
Högbom, J. A. 1974, A&AS, 15, 417
Hummel, E. 1981a, A&A, 93, 93
———. 1981b, A&A, 96, 111
Keel, W. C., & Windhorst, R. A. 1991, ApJ, 383, 135
Kellermann, K. I., & Wall, J. V. 1987, in IAU Symp. 124, Observational Cosmology, ed. A. Hewitt, G. Burbidge, & L. Z. Fang (Dordrecht: Reidel), 545
Kogut, A., et al. 1988, ApJ, 325, 1
Kogut, A., et al. 1992, ApJ, 401, 1
Koo, D. C. 1990, in ASP Conf. Ser., Vol. 10, Evolution of the Universe of Galaxies (Edwin Hubble Centennial Symposium), ed. R. G. Kron (Provo: BookCrafters), 268
Kristian, J. A., Windhorst, R. A., & Fomalont, E. B. 1993, AJ, in preparation
Kron, R. G., Koo, D. C., & Windhorst, R. A. 1985, A&A, 146, 38
Levin, S., Bensadoun, M., Bersanelli, M., De Amici, G., Kogut, A., Limon, L., & Smoot, G. 1992, ApJ, 396, 3
Lilly, S. J., Cowie, L. L., & Gardner, J. P. 1991, ApJ, 369, 79
Mandolesi, N., Calzolari, P., Cortiglioni, S., & Morigi, G. 1986, ApJ, 310, 561
Martin, H. M., & Partridge, R. B. 1988, ApJ, 324, 794
Martin, H. M., Partridge, R. B., & Rood, R. T. 1980, ApJ, 240, L79
Napier, P. J. 1989, in ASP Conf. Ser., Vol. 6, Synthesis Imaging in Radio Astronomy, ed. R. A. Perley, F. R. Schwab, & A. H. Bridle (Provo: Brigham Young Univ. Print Services), 39
———. 1992, private communication
Napier, P. J., & Rots, A. H. 1982, VLA Test Memorandum, No. 134
Neuschaefer, L. W. 1992, Ph.D. thesis, Arizona State Univ.
Neuschaefer, L. W., Windhorst, R. A., & Dressler, A. 1991, ApJ, 382, 32
Oort, M. J. A. 1987, Ph.D. thesis, Univ. Leiden
———. 1988a, A&A, 192, 42
———. 1988b, A&A, 193, 5
Oort, M. J. A., Katgert, P., Steeman, F. W. M., & Windhorst, R. A. 1987, A&A, 179, 41
Oort, M. J. A., Steemers, W. J. G., & Windhorst, R. A. 1988, A&AS, 73, 103
Oort, M. J. A., & Windhorst, R. A., 1985, A&A, 145, 405
Partridge, R. B., Hilldrup, K. C., & Ratner, M. I. 1986, ApJ, 308, 46
Pfleiderer, J. 1977, A&AS, 28, 313
Seielstad, G. A. 1983, PASP, 95, 32
Sironi, G., Limon, M., Marcellino, G., Bonelli, G., Bersanelli, M., Conti, G., & Reif, K. 1990, ApJ, 357, 301
Smoot, G. F., et al. 1990, ApJ, 360, 685
Smoot, G. F., et al. 1991, ApJ, 371, L1
Smoot, G. F., et al. 1992, ApJ, 396, L1
Subrahmanya, C. R., & Kapahi, V. K. 1983, in IAU Symp. 104, Early Evolution of the Universe and Its Present Structure, ed. G. O. Abell & G. Chincarini (Dordrecht: Reidel), 47
Tabara, H., Kato, T., Inoue, M., & Aizu, K. 1984, PASJ, 36, 297
Thompson, A. R., Clark, B. G., Wade, C. M., & Napier, P. J. 1980, ApJS, 44, 151
Thuan, T. X., & Condon, J. J. 1987, ApJ, 322, L9
Tyson, J. A. 1988, AJ, 96, 1
Wall, J. V., Benn, C. R., Grueff, G., & Vigotti, M. 1986, in Highlights Astr., Vol. 7, ed. J.-P. Swings (Dordrecht: Reidel), 345
Wieringa, M. H. 1991, Ph.D. thesis, Univ. Leiden
Wild, J. P. 1970, Australian J. Phys., 23, 113
Windhorst, R. A. 1984, Ph.D. thesis, Univ. Leiden
———. 1986, in Highlights Astr., Vol. 7, ed. J.-P. Swings (Dordrecht: Reidel), 355
Windhorst, R. A., et al. 1991, ApJ, 380, 362
Windhorst, R. A., Dressler, A., & Koo, D. C. 1987, in IAU Symp. 124, Observational Cosmology, ed. A. Hewitt, G. Burbidge, & L. Z. Fang (Dordrecht: Reidel), 573
Windhorst, R. A., Kron, R. G., & Koo, D. C. 1984b, A&AS, 58, 39
Windhorst, R. A., Mathis, D. F., & Keel, W. C. 1992, ApJ, 400, L1
Windhorst, R. A., Mathis, D. F., & Neuschaefer, L. W. 1990, in ASP Conf. Ser., Vol. 10, Evolution of the Universe of Galaxies (Edwin Hubble Centennial Symposium), ed. R. G. Kron (Provo: BookCrafters), 389
Windhorst, R. A., Miley, G. K., Owen, F. N., Kron, R. G., & Koo, D. C. 1985, ApJ, 289, 494
Windhorst, R. A., & Oppe, J. 1993, A&A, in preparation
Windhorst, R. A., van Heerde, G. M., & Katgert, P. 1984a, A&AS, 58, 1